University of Stuttgart
Germany

Faculty 6: Aerospace Engineering and Geodesy

Annual Report **2018**

Geodesy & Geoinformatics

editing and layout:
volker walter, markus antoni, martin metzner, aloysius wehr

Dear friends and colleagues,

It is our great pleasure to present to you this annual report on the 2018 activities and academic highlights of the Department of Geodesy and Geoinformatics of the University of Stuttgart. The Department consists of the four institutes:

- Institute of Geodesy (GIS),
- Institute for Photogrammetry (ifp),
- Institute of Navigation (INS),
- Institute of Engineering Geodesy (IIGS),

and is part of the Faculty of Aerospace Engineering and Geodesy.

Research

This annual report documents our research contributions in many diverse fields of Geodesy and Geoinformatics: from satellite and physical geodesy through navigation, remote sensing, engineering surveying and telematics to photogrammetry, geographical information systems and location based services. Detailed information on projects and research output can be found in the following individual institutes' sections.

Teaching

We were able to welcome 22 new BSc students in winter term 2017/2018 (initially 29 students enrolled). For the first semester of the MSc program for Geodesy and Geoinformatics 17 students enrolled. Please visit our website *www.geodaesie.uni-stuttgart.de* for additional information on the programs.

Our successful international MSc program Geomatics Engineering (GeoEngine) exists already 12 years. This time, we faced a slight decline of new students dropping from 31 last year to 22. Since we saw a similar trend also for other international MSc programs at University of Stuttgart, this is a probably a consequence of the new tuition fees for non-EU students, which have been recently established in the federal state of Baden-Württemberg.

Awards and scholarships

We want to express our gratitude to our friends and sponsors, most notably:

- Verein Freunde des Studienganges Geodäsie und Geoinformatik an der Universität Stuttgart e.V. (F2GeoS),
- Vexcel Imaging GmbH,
- Ingenieur-Gesellschaft für Interfaces mbH (IGI),
- DVW Landesverein Baden-Württemberg,

who support our programs and our students with scholarships, awards and travel support. Below is the list of the recipients of the 2018 awards and scholarships. The criterion for all prizes is academic performance; for some prizes GPA-based, for other prizes based on thesis work. Congratulations to all recipients!

Uwe Sörgel Associate Dean (Academic)
uwe.soergel@ifp.uni-stuttgart.de

Award	**Recipient**	**Sponsor**	**Programme**
Karl-Ramsayer Preis	Mr. D. Laupheimer	Department of Geodesy & Geoinformatics	Geodesy & Geo-informatics
BSc Thesis Award	Mrs. L. Joachim	F2GeoS	Geodesy & Geo-informatics
MSc Thesis Award	Mr. S. Schmohl	F2GeoS	Geodesy & Geo-informatics
Vexcel Imaging Scholarship	Mrs. L. Hong Mr. M. Shams Eddin	Vexcel Imaging	GeoEngine
Matching Funds	Mrs. C. Chen Mrs. M. Liu Mr. N. Liu	DAAD	GeoEngine

Institute of Engineering Geodesy

Geschwister-Scholl-Str. 24D
D-70174 Stuttgart
Tel.: +49 711 685 84041
Fax: +49 711 685 84044
sekretariat@iigs.uni-stuttgart.de or
firstname.secondname@iigs.uni-stuttgart.de
http://www.uni-stuttgart.de/ingeo/

Head of Institute

Prof. Dr.-Ing. habil. Volker Schwieger

Secretary

Elke Rawe
Ute Schinzel

Scientific Staff

M.Sc. Alexandra Avram	GNSS
M.Sc. Laura Balangé (since 01.12.2018)	Quality Modelling
M.Sc. Urs Basalla (since 15.10.2018)	Terrestrial Laser Scanning
M.Sc. Marko Gasparac	GNSS and Digital Map
M.Sc. Aiham Hassan	Monitoring
Dipl.-Ing. Patric Hindenberger	Location Referencing
M.Sc. Gabriel Kerekes	Terrestrial Laser Scanning
Dipl.-Ing. Otto Lerke	Machine Guidance
M.Sc. Philipp Luz (since 01.11.2018)	Digital Map
Dr.-Ing. Martin Metzner	Engineering Geodesy
M.Sc. Dung Trung Pham	Kinematic Positioning
Dipl.-Ing. Annette Scheider (until 31.03.2018)	Kinematic Positioning
M.Sc. Annette Schmitt	Multi-Sensor-Systems
M.Sc. Martin Wachsmuth	Kinematic Positioning
M.Sc. Jinyue Wang	Map Matching
Dr.-Ing. Li Zhang	Monitoring

Technical Staff

Andreas Kanzler
Martin Knihs
Lars Plate

External Teaching Staff

Dipl.-Ing. Jürgen Eisenmann	Geschäftsbereichsleiter Landratsamt Ostalbkreis, Geoinformation und Landentwicklung
Dipl.-Ing. Christian Helfert	Fachdienstleiter Flurneuordnung im Landkreis Biberach
Dipl.-Math. Ulrich Völter	Geschäftsführer der Fa. Intermetric
Dr.-Ing. Thomas Wiltschko	Daimler AG, Mercedes-Benz Cars; Research and Development

General View

The Institute of Engineering Geodesy (IIGS) is directed by Prof. Dr.-Ing. habil. Volker Schwieger. It is part of Faculty 6 “Aerospace Engineering and Geodesy” within the University of Stuttgart. Prof. Schwieger holds the chair in “Engineering Geodesy and Geodetic Measurements”. Since 2017, he is the Dean of Faculty 6.

In addition to being a member of Faculty 6, Prof. Schwieger is co-opted to Faculty 2 “Civil and Environmental Engineering”. Furthermore, the IIGS is involved in the Center for Transportation Research of the University of Stuttgart (FOVUS). Thus, the IIGS actively continues the close collaboration with all institutes in the field of transportation, especially with those belonging to Faculty 2.

Since 2011, Prof. Schwieger is a full member of the German Geodetic Commission (Deutsche Geodätische Kommission - DGK). Furthermore, he is a member of the section “Engineering Geodesy” within the DGK. He is head of the DVW working group 3 “Measurement Techniques and Systems” and chairman of the FIG Commission 5 “Positioning and Measurements” in the period from 2015 to 2018.

The institute’s main tasks in education focus on geodetic and industrial measurement techniques, kinematic positioning and multi-sensor systems, statistics and error theory, engineering geodesy and monitoring, GIS-based data acquisition, and transport telematics. Here, the institute is responsible for the above-mentioned fields within the curricula of “Geodesy and Geoinformatics” (Master and Bachelor courses of study) as well as for “GEOENGINE” (Master for Geomatics Engineering in English). In addition, the IIGS provides several courses in German for the curricula of “Aerospace Engineering” (Bachelor and Master), “Civil Engineering” (Bachelor and Master), “Transport Engineering” (Bachelor and Master) and “Technique and Economy of Real Estate” (Bachelor). Furthermore, lectures are given in English to students within the Master course “Infrastructure Planning”. Finally, eLearning modules are applied in different curricula.

In 2018 the Cluster “Integrative Computational Design and Construction for Architecture” (IntCDC), for which the university has applied for a grant as part of the excellence strategy to strengthen top-level research in Germany, has been awarded funding for the next seven years. The cluster IntCDC aims to harness the full potential of digital technologies in order to rethink design and construction, and enable groundbreaking innovations for the building sector through a systematic, holistic and integrative computational approach. As a member of the cluster (IntCDC), the institute research in the field of new construction methods is intensified in cooperation with architects, civil engineers, computer scientists, production engineers and other scientists from the university.

The current research and project work of the institute is expressed in the course contents, thus always presenting the actual state-of-the-art to the students. As a benefit of this, student research projects and theses are often implemented in close cooperation with the industry and external research partners. The main research focuses on kinematic and static positioning, analysis of engineering surveying processes and construction processes, machine guidance, monitoring, transport and aviation telematics, process and quality modelling. The daily work is characterized by intensive co-operation with other engineering disciplines, especially with traffic engineering, civil engineering, architecture, and aerospace engineering.

Research and Development

Automated Multi-sensor Early Warning System on the Three Gorges Dam - DAAD PPP China

The Project-Based Personal Exchange between the Institute of Engineering Geodesy (IIGS) at the University of Stuttgart and the School of Geodesy and Geomatics (SGG) at the University of Wuhan is supported by the DAAD (German Academic Exchange Service) and the CSC (China Scholar Council). The aim of this project is to realize an automated multi-sensor early warning system near the Three Gorges Dam. The sensors used for this purpose are GNSS, Ground Based Synthetic Aperture RADAR (GB-SAR) and Terrestrial Laser Scanner (TLS). Based on the GNSS and GB-SAR data gathered in the first measurement campaign performed in September 2017, an integration concept between both techniques was proposed. Furthermore, the atmospheric influence on the GB-SAR data was analyzed and the available correction methods were tested. The results of those tests showed that GB-SAR data are more sensitive against variation of humidity and temperature and less sensitive against variation of air pressure. The atmospheric correction of these data using Ground Control Points (GCP) is more efficient compared to the correction by means of atmospheric models based on meteorological observations gathered at the measurement site. The analysis of the displacement time series (Figure 1) at the measurement site showed no significant displacement during the measurements. The results of those investigations were published in a joint paper, written by all participants, in the FIG congress in Istanbul 2018.

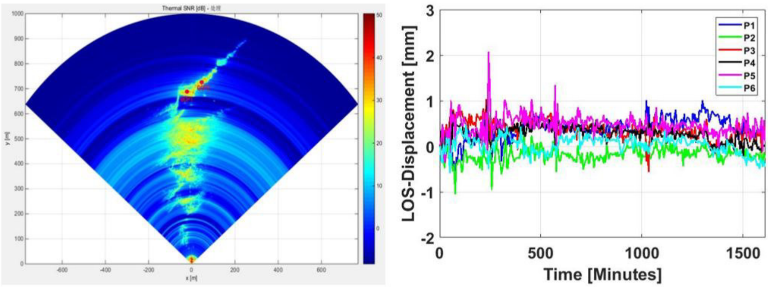

Figure 1: *SAR Thermal SNR image and selected GCPs for the atmospheric correction (left) and Line of sight (LOS) displacement time series for some pixels after atmospheric correction using GCP (right)*

In order to include TLS in the integration concept, a Bachelor thesis at the IIGS discussed the efficiency of available Laser Scanning software regarding the geodetic deformation analysis.

Prof. Volker Schwieger, Li Zhang, Annette Schmitt and Aiham Hassan visited the SGG in March 2018 and went to the Three Gorges area for the second measurement campaign. Besides the GB-SAR and GNSS measurement, TLS and low cost GNSS measurements were performed in this campaign. Within this visit, the extension of the project was discussed.

Furthermore and in order to optimize the selection of measurement configuration for the GB-SAR, a simulation was performed and the accuracy of the 3D-displacement, which can be extracted from the measured 1D LOS-displacement through a transformation involving further measurements, was analyzed under different measurement configurations. This analysis showed that the main influence factor on this accuracy is the angle between the LOS- and the real displacement directions. The results of the simulation were then approved using empirical data from the second measurement campaign. The results of this investigation were published at the GeoPreVi 2018 international symposium in Bucharest, Romania. Finally, it should be mentioned that DAAD and CSC approved the extension of the project for one year.

Adaptive Control for Guidance of Tracked Vehicles

The automatic control may be established by designing a closed-loop system, where the process respectively the plant follows a reference variable, respectively a set point. The main disadvantage of conventional controllers (3-point-, PID-, or Fuzzy- controllers) is that during changes in the environment (or the process) the controller parameters need to be retuned and reset to keep the control quality at a desirable level. To overcome this drawback, an adaptive controller can be used which automatically adjusts in particular alternating operating conditions in order to match the set requirements on control quality.

Among different adaptive controller schemes, the self-tuning regulators and controllers (STR/ STC) have been chosen for guidance of a tracked UGV.

The starting point is an ordinary closed-loop system, where the feedback signal is processed within a controller in order to minimize the control deviation. This feedback control loop is now extended by an additional functionality, which identifies the controlled process by the use of its input and output. The extension estimates the process parameters and subsequently calculates the controller settings, respectively its parameters.

The online parameter estimation, related to the identification step, is based on a linear model, expressed as linear difference equation in the shape of an ARMAX model (autoregressive moving average model with auxiliary or exogenous input).

$$y(t) + a_1 y(t-1) + \cdots + a_n y(t-n) = b_0 u(t-k) + b_1 u(t-k-1) + \cdots$$
$$\ldots + b_m u(t-k-m) + c_0 \xi(t) + c_1 \xi(t-1) + \cdots + c_n \xi(t-n) + d(t) \qquad (1)$$

y - controlled variable, u - regulating variable, a_i, b_i, c_i - model parameters, ξ - stochastic noise, d - disturbance variable (not measured).

After the process model parameters have been estimated, the calculation of suitable controller settings for control action must be performed. The minimum variance control law can be derived by rearrangements and simplifications of equation (1) in order to obtain the regulating variable (Seborg et al. 1986):

$$u(t) = \frac{1}{\beta_0}\big(\alpha_1 y(t) + \cdots + \alpha_n y(t-n+1)\big) - \beta_1 u(t-1) - \cdots - \beta_l u(t-l) \qquad (2)$$

Exemplarily, four driving experiments have been conducted, whereas two of them have taken place in laboratory and two under outdoor conditions. The achieved results are satisfactory, while showing the control quality of the STC at a comparable level to the conventional PID controller under laboratory conditions (Table 1). The outdoor experiments show a better performance of the STC (Table 2).

Table 1: *RMS values for the laboratory experiments*

Trajectory	Self-tuning controller (STC)	PID controller
1 (oval)	*0.0023 m*	*0.0018 m*
2 (eight)	*0.0037 m*	*0.0028 m*

The greatest advantage of adaptive controllers is the non-necessity of excessive, time-consuming tuning procedures and the indicated better performance in outdoor driving environments.

Table 2: *RMS values for the outdoor experiments*

Trajectory	Self-tuning controller (STC)	PID controller
3	*0.0089 m*	*0.0131 m*
4	*0.0072 m*	*0.0086 m*

Optimization of the Positioning of Adaptive Supports

At the university of Stuttgart, the first adaptive double curved plane load bearing structure was developed. This structure is called Stuttgart SmartShell. It has got a base area of about 100 m_2 and a thickness of 4 cm, made of multilayer wood. Resting on three adaptive supports and one static support, the Stuttgart SmartShell offers the investigation of possibilities to reduce stress and structural vibration, while the weight of the structure is reduced drastically. Figure 2 shows the Stuttgart SmartShell.

In a former investigation, laser scanning data from 2012 were compared with a data set from 2015 of the initial position. The two data sets were transformed as well and compared. This comparison shows significant deviations at one support. Reasons for those deviations could be the ageing of the structure and the influence of the weather. These deviations led to a fracture of the structure. After fixing the structure, a new CAD model was created from laser scanning data.

The optimization of the position of the adaptive support due to environmental influences is the main task of this project. The deviations due to the environmental influences are investigated by laser scanners. To detect the significant deviations it is necessary to know the 3D-point error of the measured points. This error is calculated for a complete scan of the Stuttgart SmartShell by using the synthetic variance covariance matrix from IMKAD. In the next step, an algorithm to compute the deformation analysis is developed based on the 3D - point errors and the law of error propagation.

Figure 2: *Stuttgart SmartShell (© Bosch Rexroth)*

Quality assurance for wooden pavilion

For the Bundesgartenschau 2019 in Heilbronn, the Institute for Computational Design and Construction (ICD) has planned a wooden pavilion. Similar to the pavilion of the Landesgartenschau 2014 in Schwäbisch Gmünd, it is constructed with many wooden elements. These wooden elements, called cassettes, are made of spruce wood glued together. For this pavilion, the plan is that the cassettes fit with small tolerances, meaning the cassettes are milled to the true form and not smaller. The aim is to investigate how precise the milling process of the cassettes is. Therefore it is planned to take measurements with the API laser tracker along the edges that are in contact with other elements. These measured edges will then be compared to the CAD model of the equivalent cassette (Figure 3). In December, two measurements took place and further measurements are planned. Furthermore, scanning of the whole pavilion is planned in three stages: after constructing, midterm and before deconstructing.

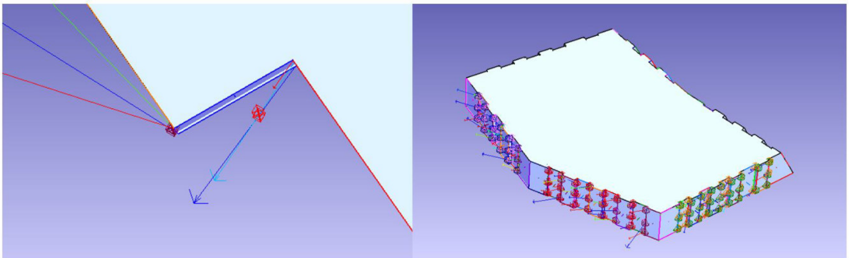

Figure 3: *CAD model of a wooden cassette with laser tracker measurements.*

For the Remstal Gartenschau 2019, the ICD has planned a wooden tower. Half of the wooden elements will be constructed in Switzerland. These wooden elements will be constructed with curved wood bilayers. The approximately 30 curved wood bilayers will be scanned at the factory “Blumer-Lehmann” in Gossau (CH) to obtain the radii. In a next step, the wood bilayers will be glued into two fifteen meter long elements. These will be scanned as well at the factory. Of these larger elements the finished components will be milled out and scanned again at the factory. The plan is to build the tower near Urbach and have it scanned every six months for monitoring purposes. The tower is planned to be on site for five years.

Hybrid model for GNSS multipath simulation

Errors in the GNSS receiver Delay-Locked Loop (DLL) and Phase-Locked-Loop (PLL) are mainly caused by multipath biased phase and code measurements. These influence the positioning algorithms and induce errors in the final coordinates. In order to analyse the receiver tracking error for a specific environment with a GNSS (Global Navigation Satellite System) signal generator, a combination between a deterministic and a statistic model is used. A deterministic model is appropriate when the system is well known, whereas a statistic one describes the unknowns in terms of probabilities. Considering that GNSS multipath errors are influenced by many factors, a combined model is appropriate to describe the system accurately.

The Fresnel-Kirchhoff formula is implemented to model the diffraction in 2D. Given the satellite elevation angle, building coordinates, antenna position and height, the signal fading characteristics are modelled. Diffuse multipath is added to the time series to take into account the random scattering. For this purpose, a Rayleigh fading channel using Gaussian distributions in quadrature is implemented. The 2D environment is modelled and the signal fading is simulated for a satellite at 35° elevation.

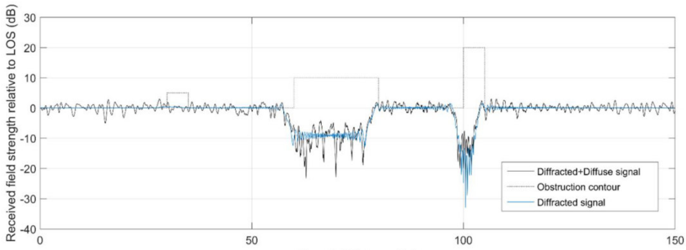

Figure 4: *MATLAB simulation of the 2-dimensional environment and the corresponding multipath series for one satellite at 35° elevation. The receiving antenna is simulated along a trajectory parallel to the three buildings*

Figure 4 shows the three buildings, which are modelled. The corresponding multipath fading is outlined with the black line along the trajectory, whereas the blue line represents the diffraction. It is visible that the higher the building, the more affected is the signal. This approach is appropriate for multipath simulations, where a specific environment has to be considered.

Integrated space-time modelling based on correlated measurements for the determination of survey configurations and the description of deformation processes (IMKAD II)

Gefördert durch DFG Deutsche Forschungsgemeinschaft

The previous DFG (Deutsche Forschungsgemeinschaft) project IMKAD I focused on functional modelling of point clouds, stochastic modelling of terrestrial laser scanners' (TLS) error sources and analyzing survey configurations for space-continuous monitoring. The advances obtained during the IMKAD I project, but also the drawbacks of different measurements are subject to deeper research in the current proposal.

In recent years, B-spline curves and surfaces became popular within engineering geodesy due to their suitability in representing point cloud information. However, if geometry is functionally modeled through local B-spline and global Bézier surfaces without stochastic information about the control points, this may lead to unrealistic surface estimations. The approach developed in collaboration with the Austrian partner Research Group Engineering Geodesy (RGEG) from TU Wien foresees the use of a synthetic covariance matrix to stochastically model TLS point clouds. This is further used as weighting information in the B-spline model:

$$\boldsymbol{\Sigma}_{ll} = \sum_{k=1}^{p} \boldsymbol{D}_k \cdot \boldsymbol{\Sigma}_{\delta\delta,k} \cdot \boldsymbol{D}_k^T + \boldsymbol{F} \cdot \boldsymbol{\Sigma}_{\xi\xi} \cdot \boldsymbol{F}^T + \sum_{h=1}^{q} \boldsymbol{G}_h \cdot \boldsymbol{\Sigma}_{\gamma\gamma,h} \cdot \boldsymbol{G}_h^T$$

With p matrices D_k for non-correlating errors, one matrix F for functional correlating errors, q matrices G_h for stochastic correlating errors. $\Sigma_{\delta\delta,k}$ the covariance matrix for the non-correlating errors, $\Sigma_{\xi\xi}$ the covariance matrix for the functional correlating errors, $\Sigma_{\gamma\gamma,h}$ the covariance matrix for the stochastic correlating errors. Until now, this model was developed for a phase-based panoramic scanner (Leica HDS 7000) and not validated through real-world measurements. The future steps imply the creation of an extended synthetic covariance matrix with an improved functional model for the phase-based scanner and a new model for a pulse-based scanner (Riegl VZ-2000). Furthermore, validation experiments are planned for objects that range in dimension from 30 cm (laboratory conditions) up to 300 m (water dam). As regards findings, we expect to achieve a realistic stochastic model for point clouds and determine optimal scanning parameters for deformation analysis based on B-spline surface estimation.

Ghosthunter - Telematics System against Ghost Drivers using GNSS

The aim of the Ghosthunter II research project is to develop a detection system to extend current car navigation systems detecting ghost drives on motorways and their ramps and warning both the ghost drivers themselves and other road users. This project is carried out in cooperation with the Institute of Space Technology and Space Applications at the University of the Federal Armed Forces Munich and the companies NavCert and TomTom.

Supported by:

Federal Ministry for Economic Affairs and Energy

on the basis of a decision by the German Bundestag

In a first step, the algorithms developed in the previous project must be ported and optimized with regard to the lower performance of the target hardware. The TomTom Bridge navigation system based on Android was selected as the target hardware.

In order to ensure the real-time capability of the algorithm, changes have been made. Especially the search functions and the data structure have been improved. Thus it was possible to reduce the time to match a GPS position from 1460 ms to 400 ms. Furthermore, an Android app was developed to visualize the digital map as well as the results of the map matching and to allow an operation in the car (Figure 5).

The next steps include the integration of traffic flow data and the adaptation of the algorithm to lane exact ADAS maps. In addition, the integrity of the system will be analyzed.

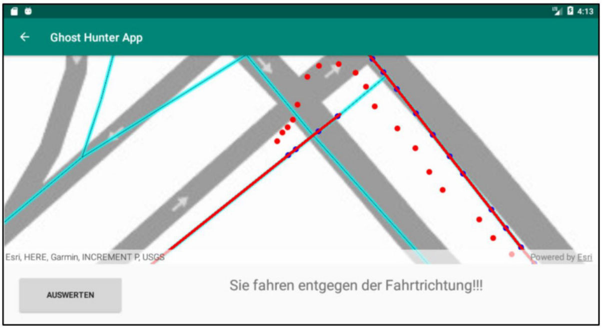

Figure 5: *Interface of the Android App "Ghosthunter"*

TransSec - Autonomous Emergency Manoeuvering and Movement Monitoring for Road Transport Security

With the rise of truck-based terror attacks in European countries (like in Nice and Berlin), a new form of transport security is necessary to help prevent such incidents. For this purpose, a European Project TransSec (Autonomous emergency manoeuvering and movement monitoring for road transport security) is funded by the European Commission within the program Horizon H2020 for three years. This project was started in February 2018 and its goal is to design and implement such an intelligent positional monitoring and manoeuvering system to prevent terror attacks.

The Institute of Engineering Geodesy (IIGS) at the University of Stuttgart is one of the five partners involved in the TransSec project. The IIGS has the task to design, develop and implement a prototype of map including the static environment as well as an electronic horizon provider for the vehicle based on a map aiding algorithm. Finally, a local dynamic map will be created using the information of the current acquired situation from the sensors like cameras and laser scanners, so that the dynamic objects like vehicles, pedestrian around the trucks can be detected.

And the other task of IIGS is to get the precise positioning of the trucks by integrating the data from GNSS and other additional sensors like odometer, gyroscopes and accelerometers, cameras and Lidar, etc.

In 2018, map data availability and quality analysis was done. The first demonstration of positioning system (based on GNSS only) with map preview was successful. The next step is the extension of the static map and multisensor integration.

Dynamic Location Referencing: Probability and Fuzzy Logic based decision systems

Dynamic Location Referencing is a well-known methodology to transfer geoobjects from one digital road map to another in such cases where no common databases and/or common structures are available and are typically used to share traffic information. The key issue in dynamic Location Referencing is to find the correct geoobject in the target map which corresponds to the geoobject in the source map. So far, in nearly all methods an analytical (deterministic) algorithm is implemented to perform this. Given the fact that geodata as well as the matching procedure for geodata has some uncertainty, it is obvious to research uncertainty-based algorithms.

For this, two different uncertainty-based approaches were picked up and investigated in detail. Firstly, a probability-based approach, for which a corresponding decision algorithm was formulated using the already estimated probability distributions for a given set of criteria (geometrical, topological, syntactical and semantical). Secondly, a fuzzy-based approach by defining the fuzzy sets for the input criteria (same set of criteria like for probability-based) and the output criterion (grade of correspondence), specifying the rule base, fuzzy inference system and defuzzification strategy. For the latter, various optimizations were carried out to determine the best methods (fuzzy logical operations, defuzzification method).

To evaluate the performance, a QGIS-based module has been developed implementing these two approaches and extended by the well-known analytical OpenLR-algorithm to compare the results between the uncertainty-based and determined concepts. A first evaluation has been done by using real live traffic situations in the city of Stuttgart and selecting the underlying edges in the digital maps of TomTom and HERE. These selected edges have been transferred from TomTom to HERE and vice versa to compare the results for the specific mapping direction based on the same traffic situation. As a result, the probability-based and fuzzy-based approaches show similar results with an average hit rate up to 90% (nearly equal for both mapping directions) and improve the results of OpenLR in average by 12 percentage points.

In conclusion, the uncertainty-based algorithms deliver an adequate performance and thus offer an alternative to the analytical algorithms, promising a significant improvement of the results in an expected range of 10 percentage points.

Selection of a filter algorithm non-linear problem definition

For the estimation of trajectories a suitable non-linear filter algorithm (Extended Kalman Filter, Unscented Filter, Particle Filter) shall be applied. The optimal filter can be evaluated according to different criteria, whereby the easiest way to evaluate the optimal algorithm is to use the difference between a true and an estimated trajectory. However, since the true trajectory is usually not available, alternative approaches are used to assess the quality of the filter. In a study, an optimal filter algorithm was selected on the basis of a nonlinearity measures. By means of examples for the selection of the filter algorithm it becomes clear that nonlinearity provides a criteria approach for the selection of an optimal filter model.

Position Determination of a Moving Reflector in Real Time by Robotic Total Station Angle Measurements

Angle readings from Robotic Total Stations (RTS) can be acquired with a higher update rate in comparison to distance measurements. For short ranges, these readings can be considered more accurate than the distance measurements. The currently presented system combines measurements from two Leica RTS (TS30 and TS16) that have Automatic Target Recognition (ATR) sensors. This helps at identifying and tracking the reflector. Both RTS are stationed in the same coordinate reference frame and controlled by a central computer running a LabVIEW program. It retrieves the angle measurements via GeoCOM protocols and computes the current position of the moving reflector based solely on angle intersection principles, similar to a Theodolite Measurement System (TMS) (Figure 6). This increases the positioning frequency of the RTS system to 20 points/second, which is twice as fast as the normal tracking mode of these specific RTS. A miniature railway and trolley are used to move the studied reflectors in laboratory experiments with ranges of up to 6 m.

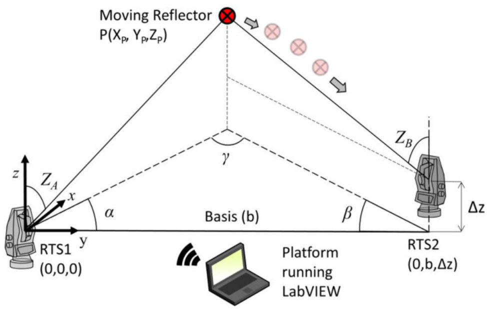

Figure 6: *System components with measured and computed values*

Firstly, different angle based positions of each reflector are compared to positions that result from measurements of angles and distances for the same points while the trolley is stationary. The differences are under 1 mm, confirming that the implemented mathematical model is correct. Further experiments present the achieved positions in kinematic mode (at slow speeds) by means of lateral deviations to a reference line. Results show an average lateral deviation of 2.1 mm for the two 360° reflectors and 3.3 mm for a normal reflector (Figure 7). Here, synchronization of the two RTS readings is the most significant factor.

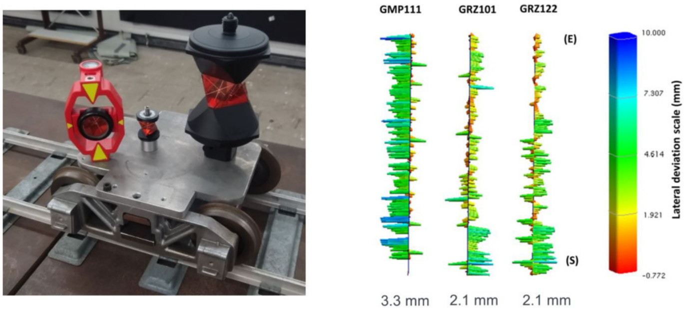

Figure 7: *Reflectors on trolley (from left to right - GMP111, GRZ101, GRZ122); lateral deviation for each scenario/reflector (right)*

Kinematic Positioning in a Real Time Robotic Total Station Network System

A network of Robotic Total Stations (RTSs) facilitates continuous tracking of a moving reflector even when obstructions interfere with the line-of-sight. Further on, a representative system comprised of two Leica RTSs (TS30 and TS16) is presented. These are stationed in the same coordinate frame and track one 360° reflector in a synchronized manner. If one line-of-sight is interrupted, the specific RTS is set to a passive state and will continue to "blindly" track the reflector until a new line-of-sight is available. In guidance and control applications, having one RTS limits the positioning accuracy to the instrument's technical specifications and narrows down the area of use. Multiple networked RTSs (Figure 8 left), on the other side, enhance the accuracy through an optimal measurement configuration and assure a non-interrupted tracking process. A central computer establishes multidirectional data flow between each RTS with the help of the Leica GeoCOM Protocol and a LabVIEW based program. During the active tracking phase, each calculated position is stored and simultaneously made available for all other instruments in the network.

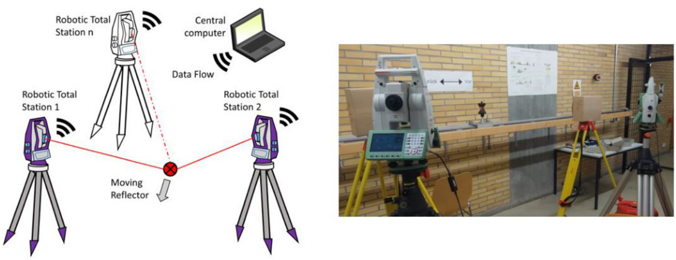

Figure 8: *Real Time Robotic Total Station Network System (left), experimental setup (right)*

To verify the system's performance, a reflector is fixed on trolley and measured while travelling with constant speed on a calibration rail (Figure. 8 right). The boxes interrupt the line-of-sight for each RTS in a controlled manner, thus creating areas where both or only one RTS are either in active or passive state. The rail serves as line of reference with coordinates determined by a laser tracker. Lateral deviations to this line are considered quality indicators for the tracking process.

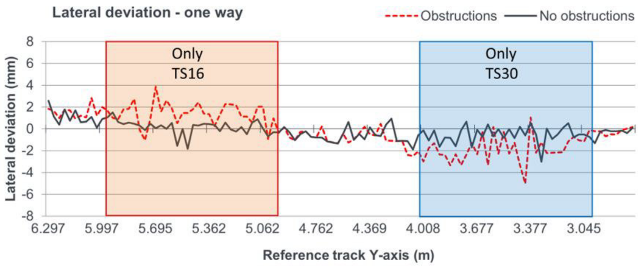

Figure 9: *Lateral deviation of the 360° reflector position with respect to a reference line (0)*

As briefly shown in Figure 9, the RTS network system reduces the lateral deviation (middle area and continuous line), improves the positioning accuracy in tracking mode and generally increases reliability.

Publications

Refereed Publications

Abdallah; A.; Schwieger, V: Improving Hydrographic PPP by Height Constraining. FIG Congress 2018, Istanbul, Turkey. May 06-11, 2018.

Aichinger, J., Schwieger, V.: Influence of scanning parameters on the estimation accuracy of control points of B-spline surfaces, Journal of Applied Geodesy, 12 (2), pp. 157-167, deGruyter, Berlin, 2018.

Avram, A.; El Gemayel, N.; Schwieger, V.: Assessment of the Delay-Locked Loop error due to multipath models regarding a deterministic-stochastic channel and a GPS L1 receiver model for kinematic trajectories. Proceedings of the 31st International Technical Meeting of the Satellite Division of the Institute of Navigation (ION GNSS+ 2018), September 24 - 28, 2018.

Hassan, A., Xu, J., Xing, C., Schwieger, V. (2018): A contribution to variance analysis of 3D-displacement extracted from GB-SAR measurements. GeoPreVi International Symposium, 29-30 October 2018, Bucharest, Romania.

Kerekes, G., Schwieger, V.: Kinematic Positioning in a Real Time Robotic Total Station Network System. 6th International Conference on Machine Control and Guidance. Bornimer Agrartechnische Berichte Heft 101, ISSN 0947-7314, p. 35-43, Berlin, Germany.

Kerekes, G., Schwieger, V.: Position Determination of a Moving Reflector in Real Time by Robotic Total Station Angle Measurements. GeoPreVi International Symposium, 29. - 30. October, 2018, Bucharest, Romania.

Lerke, O., Schwieger, V.: Adaptive Control for Guidance of Tracked Vehicles. 6th International Conference on Machine Control and Guidance. In Bornimer Agrartechnische Berichte Heft 101, ISSN 0947-7314, p. 83-94, Berlin, Germany.

Zhang, L.; Ionescu, I.-M., Schwieger, V.: Monitoring of the church tower in Herrenberg with Low-Cost GNSS. GeoPreVi International Symposium, 29-30 October 2018, Bucharest, Romania.

Non-Refereed Publications

Hassan, A., Xu, J., Zhang, L., Liu, G., Schmitt, A., Xing, C. Xu, Y., Ouyang, C., Schwieger, V.: Towards integration of GNSS and GB-SAR measurements: Exemplary monitoring of a rock fall at the Yangtze River in China. FIG CONGRESS 2018, Istanbul, Turkey.

Hindenberger, P.; Schwieger, V.: Probability Based Location Referencing Method - Statistical Evaluations and Estimated Probability Distributions. 14th Conference on Location Based Services (LBS), Zurich, Switzerland, January 15-17, 2018.

Wang, J.; Wachsmuth, M.; Metzner, M.; Schwieger, V.: Die digitale Karte als Sensor. 176. DVW-Seminar Multisensortechnologie: Low-Cost Sensoren im Verbund (MST 2018), Hamburg.

Monographs, books and book chapters

Schwieger, V.; Beetz, A.: Baumaschinensteuerung - der ingenieurgeodätische Beitrag, pp. 283-318. In: Schwarz, W. (Hrsg.): Ingenieurgeodäsie, Springer, Berlin, 2017.

Wieser, A.; Kuhlmann, H., Schwieger, V., Niemeier, W.: Ingenieurgeodäsie - eine Einführung, pp. 1-22. In: Schwarz, W. (Hrsg.): Ingenieurgeodäsie, Springer, Berlin, 2017.

Presentations

Schwieger, V.: Integrated Monitoring of a Rockfall at the Yangtse River. Interexpo GeoSiberia 2018, Novosibirsk, Russia, April 24-26, 2018.

Schwieger, V.: Positioning for Autonomous Driving. FIG Congress 2018, Istanbul, Turkey. May 06-11, 2018.

Schwieger, V.: Punktwolken - warum, wie und wofür? 12. GeoMessdiskurs, Jena, 28.06.2018.

Schwieger, V.: Automatisiertes Fahren und Geodäsie. Tübingen, Wildermuth Gymnasium, 28.09.2018.

Schwieger, V.: Geodesy for Smart Construction. GeoPreVi 2018, Bucharest, Romania, October 29 - 30, 2018.

Schwieger, V.: Map Matching Applications. Seminar SE 3.05 "GPS/INS-Integration und Multisensor-Navigation", Carl-Cranz-Gesellschaft e.V., Oberpfaffenhofen, 22.11.2018.

Zhang, L.: Monitoring of Rock Fall at Yangtze River with Low-Cost GNSS receiver. Second workshop of DAAD Thematic Network Modern Geodetic Space Techniques for Global Change Monitoring, 24.-28. 07 2018, Luxembourg.

Zhang, L.: Low-Cost GNSS for geodetic applications. FIG Congress 2018, 06.-11.05.2018, Istanbul, Türkei.

Activities at the University and in National and International Organisations

Volker Schwieger

Dean of the Faculty of Aerospace Engineering and Geodesy, University of Stuttgart
Full member of the German Geodetic Commission (Deutsche Geodätische Kommission - DGK)
Member of the section "Engineering Geodesy" within the German Geodetic Commission (DGK)
Chair of FIG Commission 5 "Positioning and Measurement"
Head of Working Group III "Measurement Methods and Systems" of Deutscher Verein für Vermessungswesen (DVW)
Chief Editor of Peer Review Processes for FIG Working Weeks and Congresses
Member of Editorial Board Journal of Applied Geodesy
Member of Editorial Board Journal of Applied Engineering Science
Member of Editorial Board Journal of Geodesy and Geoinformation

Martin Metzner

Member of the NA 005-03-01 AA "Geodäsie" at the DIN German Institute for Standardization

Li Zhang

Co-Chair of FIG Commission 5 (Positioning and Measurement), Working Group 5.6

- Cost Effective Positioning
Member of Working Group III “Measurement Methods and Systems” of Deutscher Verein für Vermessungswesen (DVW)

Doctorates

Glabsch, Jessica: Konzeption und Realisierung kosteneffizienter GNSS-Monitoring - Systeme für ingenieurgeodätische Überwachungsmessungen Hauptberichter: Prof. Dr.-Ing. Otto Heunecke, Mitberichter: Prof. Dr.-Ing. habil. Volker Schwieger

Kemper-Böninghausen, Rolf: Entwicklung automatisierter Messverfahren für Vortriebskontrollen beim Rohrvortrieb Hauptberichter: Prof. Dr.-Ing. habil. Wolfgang Niemeier, Mitberichter: Prof. Dr.-Ing. habil. Volker Schwieger

Master Theses

Abuwarda, Amgad: Performance Analysis of a Topological Weight-Based Map-Matching Algorithm with Real Vehicle Positioning Data (Wang)

Basalla, Urs: Zielverfolgung mittels von Leica TS16 erfassten Objektbildern (Kerekes)

Bolocan, Alin: Investigation of the behaviour of Terrestrial Laserscanner beams due to wood (Schmitt)

El Ankh, Salih: Development of availability forecasts for GPS visibility along railway tracks (Metzner)

Fuchs, Florian: Realisierung einer Gridmap basierend auf Sensordaten zur Verifizierung der Umfelderfassung (Metzner)

Ionescu, Iuliana-Madalina: Monitoring of the church tower in Herrenberg with GNSS (Zhang)

John, Jelin: Implementation of an Inertial Measurement Unit for Determining the Orientation within the Control Algorithm of a Model Dozer (Lerke)

Liu, Zhixin: Implementation of real-time map-matching algorithms with a Windows based C++ development environment (Wang)

Luz, Philipp: Positionsbestimmung und Navigation mittels bildverarbeitender Tachymeter (Lerke)

Mahr, Sabine: Nick- und Wankwinkelschätzung des Eigenfahrzeugs für radarbasierte Assistenzsysteme (Lerke)

Mendoza, Kevin Para: Displacement and deformation detection of a model structure simulated by a mechanical actuator using the Leica HDS7000 laser scanner (Kerekes)

Ren, Wenhao: Untersuchung von Odometern auf Eignung als Positionssensoren zur Überbrückung von Messunterbrechungen des Tachymeters aufgrund von Sichtbehinderungen (Lerke)

Schneider, Patrick: Entwicklung einer Koppelnavigation für den Nutzfahrzeugbereich (Gasparac, Metzner)

Stilling, Niclas: Erstellung und Umsetzung eines prototypischen Kalibrierkonzepts und Justagekonzepts für Radarsensoren an Agrar- und Baumaschinen (Schwieger)

Zhao, Yuzhe: Bestimmung einer GNSS Kombinationslösung aus mehreren individuellen GNSS-Messungen für die Absteckung hoher Türme (Zhang)

Bachelor Theses

Ganesharatnam, Marien: Analyse der Wertschöpfungskette im kombinierten Flurneuordnungsverfahrens Uttenweiler (B 312) (Helfert, Metzner)

Hörz, Joachim: Reaktivierung innerörtlicher Flächen zur Senkung des Flächenverbrauchs (Helfert, Metzner)

Rahn, Anne: Analyse der Eignung verfügbarer Laserscanning-Softwarepakete für die geodätische Deformationsanalyse natürlicher und künstlicher Objekte (Hassan)

Keller, Philipp: Untersuchung des Messverhaltens der Lineareinheit des IIGS (Schmitt)

Tsao, Wen-Ning: Optimierung von Messkonzepten für Deformationsanalyse mittels JAG3D (Schmitt)

Wang, Rui: Deformationsanalyse einer Staumauer mit GNSS (Zhang, Lerke)

Education

SS18 and WS18/19 with Lecture/Exercise/Practical Work/Seminar

Bachelor Geodesy and Geoinformatics (German)

Basic Geodetic Field Work (Wachsmuth, Kanzler)	0/0/5 days/0
Engineering Geodesy I (Schwieger, Kerekes)	4/2/0/0
Geodetic Measurement Techniques I (Metzner, Wachsmuth)	3/1/0/0
Geodetic Measurement Techniques II (Schmitt)	0/1/0/0
Integrated Field Work (Kerekes, Metzner)	0/0/10 days/0
Methods of Measurements and Analysis in Engineering Geodesy (Schwieger, Kerekes)	2/2/0/0

Reorganisation of Rural Regions (Helfert)	1/0/0/0
Statistics and Error Theory (Schwieger, Wang)	2/2/0/0

Master Geodesy and Geoinformatics (German)

Causes of Construction Deformation (Metzner, Wang)	1/1/0/0
Deformation Analysis (Zhang)	1/1/0/0
Industrial Metrology (Schwieger, Schmitt, Kanzler)	1/1/0/0
Land Development (Eisenmann)	1/0/0/0
Monitoring Measurements (Schwieger, Basalla)	1/1/0/0
Monitoring Project (Schmitt)	0/0/2/0
Terrestrial Multisensor Systems (Zhang, Lerke, Kerekes)	1/1/0/0
Thematic Cartography (Zhang, Lerke)	1/1/0/0
Transport Telematics (Zhang, Luz)	2/2/0/0

Master GeoEngine (English)

Integrated Field Work (Kerekes, Metzner)	0/0/10 days/0
Kinematic Measurement Systems (Schwieger, Lerke)	2/2/0/0
Monitoring (Schwieger, Wang)	1/1/0/0
Thematic Cartography (Zhang, Basalla)	1/1/0/0
Transport Telematics (Metzner, Luz, Balangé)	2/1/0/0
Terrestrial Multisensor Systems (Zhang, Schmitt)	2/1/0/0

Bachelor and Master Aerospace Engineering (German)

Statistics for Aerospace Engineers (Zhang, Hassan)	1/1/0/0

Master Aerospace Engineering (German)

Industrial Metrology (Schwieger, Schmitt, Kanzler)	1/1/0/0
Transport Telematics (Zhang, Luz)	2/2/0/0

Bachelor Civil Engineering (German)

Geodesy in Civil Engineering (Metzner, Hassan)	2/2/0/0

Master Civil Engineering (German)

Geoinformation Systems (Metzner, Hassan)	2/1/0/0
Transport Telematics (Zhang, Luz)	2/1/0/0

Bachelor Technique and Economy of Real Estate (German)

Acquisition and Management of Planning Data and Statistics (Metzner, Kanzler)	2/2/0/0

Bachelor Transport Engineering (German)

Statistics (Metzner, Kanzler)	0.5/0.5/0/0
Seminar Introduction in Transport Engineering (Schmitt)	0/0/0/1

Master Infrastructure Planning (English)

GIS-based Data Acquisition (Zhang, Schmitt)	1/1/0/0

Institute of Geodesy

Geschwister-Scholl-Str. 24D
D-70174 Stuttgart
Tel.: +49 711 685 83390
Fax: +49 711 685 83285
gis@gis.uni-stuttgart.de
http://www.gis.uni-stuttgart.de

Head of Institute

Prof. Dr.-Ing. Nico Sneeuw

Emeritus

em. Prof. Dr.-Ing. habil. Dr. tech. h. c. mult. Dr.-Ing. E. h. mult. Erik W. Grafarend

Academic Staff

Dr.-Ing. Markus Antoni	Physical Geodesy, Satellite Geodesy
Dr. Karim Douch (since 21.3)	Physical Geodesy, Seismology
M.Sc. Omid Elmi	Remote Sensing
PD Dr.-Ing. habil. Johannes Engels	Physical Geodesy, Satellite Geodesy
Dr. Hassan Hashemi Farahani (since 1.3)	Physical Geodesy, Satellite Geodesy
Prof. Dr. sc. techn. Wolfgang Keller (until 28.9)	Physical Geodesy, GNSS
Dr.-Ing. Friedrich Krumm	Adjustment Theory, Mathematical Geodesy

Research Associates

M.Sc. Sajedeh Behnia	Satellite Altimetry
M.Sc. Muhammad A. Javaid	Satellite Geodesy
M.Sc. Wei Liu	Satellite Geodesy
M.Sc. Saemian Peyman	Satellite Geodesy, Hydrology
M.Sc. Shirzad Roohi (until 27.5)	Satellite Altimetry, Hydrology
Dr.-Ing. Bramha Dutt Vishwakarma	Hydrology, Filter Methods
Dipl.-Ing. Elisabeth Woisetschläger (until 9.5)	Satellite Geodesy, Altimetry, Hydrology

PhD Zhi Yin	Geodynamics, Physical Geodesy
M.Sc. Jinwei Zhang	Geodetic Data Analysis

Administrative/Technical Staff

Dipl.-Ing. (FH) Thomas Götz	IT System, Controlling
Dipl.-Ing. (FH) Ron Schlesinger	IT System, Technical Support, Gravimetry
Anita Vollmer	Secretary

External Lecturers

Dipl.-Ing. Steffen Bolenz	Stadtmessungsamt, Stuttgart
Dipl.-Ing. Gerhard Grams	Ministerium für Ländlichen Raum und Verbraucherschutz Baden-Württemberg, Stuttgart
Dipl.-Ing. Dieter Heß	Ministerium für Ländlichen Raum und Verbraucherschutz Baden-Württemberg, Stuttgart

Guests

Prof. Andrzej Borkowski	Wrocław University of Environmental and Life Sciences, Wrocław, Poland (24–27.4)
Assoc. Prof. T Fukushima	National Astronomical Observatory of Japan (NAO), Tokyo, Japan (3–7.9)
Prof. Dr. Elsayed Issawy	National Research Institute of Astronomy and Geophysics Helwan, Egypt (18–29.6)
MSc student Weijie Li	Tongji University, Shanghai, China (1.4–30.9)
Assoc. Prof. Yi Lin	Tongji University, Shanghai, China (29.7–12.9)
Prof. Yunzhong Shen	Tongji University, Shanghai, China (26.11)
PhD student Kaihua Wang	University of Wuhan, Wuhan, China (1.4–30.9)
Junior Researcher Wei Wang	CASM, Beijing, China (1.9.18–27.2.19)
PhD student Yongqi Zhao	University of Wuhan, Wuhan, China (1.4–30.9)
PhD student Tinghui Zhang	Tongji University, Shanghai, China (1.9.18–28.2.19)

Research

Gravitational Field of Comet 67P/Churyumov-Gerasimenko

A field that fulfills the Laplace equation is harmonic, i.e., both source-free and curl-free. Despite the good performance on solving the gravitational field generated by spheroidal bodies (e.g., the Earth), the series may be divergent inside the Brillouin sphere enclosing all field-generating mass. Divergence may occur when determining the gravitational fields of asteroids or comets that have complex shapes, which is known as the Complex-Boundary Value Problem (CBVP). To overcome this weakness, we propose a new numerical method based on the well-known equivalence transformation, in which a potential-flow velocity field and a gravitational force vector field are equivalent in a mathematical sense, both referring to a harmonic vector field. The governing equation and the boundary condition of potential flow are derived as an alternative of Laplace's equation. Correspondingly, the computational fluid dynamics (CFD) techniques are introduced as a numerical solving scheme.

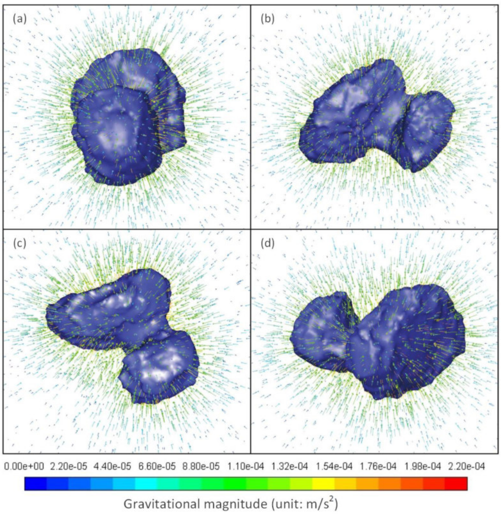

Figure 1: The gravitational vector field of comet 67P.

This project applies the novel approach to the gravitational field of comet 67P/Churyumov-Gerasimenko with a complex shape, and the result is visualized with the vectors (Figure 1), the plumb lines (Figure 2) and the scalar surface gravitation (Figure 3), respectively. The numerical scheme adopted in this method is able to overcome the divergence problem and has a good performance on solving the CBVPs.

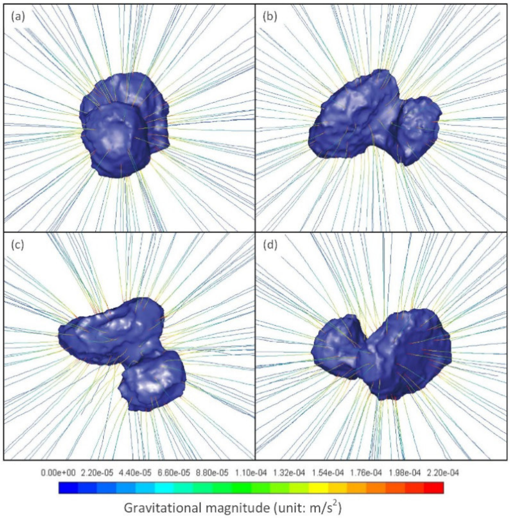

Figure 2: The plumb lines of comet 67P.

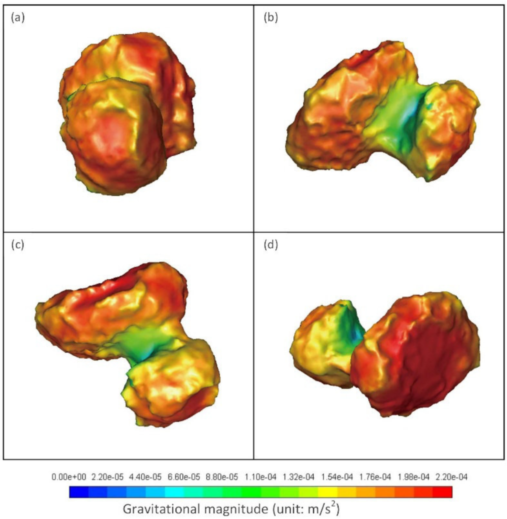

Figure 3: The surface scalar gravitation of comet 67P.

Two-step aliasing mechanism of ocean tides in satellite gravimetry

Ocean tides are undersampled in satellite missions because of their high frequencies. Therefore, aliasing occurs. Aliasing problems are deeply and widely investigated in satellite altimetry. In comparison, the aliasing of ocean tides in satellite gravimetry called enough attention in past decades, but the understanding is not systematic and comprehensive.

On one hand, the ocean tide aliasing in satellite gravimetry and in satellite altimetry are all undersampled by orbits. On the other hand, they are different in several aspects:

- Altimetry satellites are usually in repeat orbits, while gravimetry satellites are not;
- The results derived from satellite altimetry are 'point-wise' or locally averaged, while the fields derived from satellite gravimetry are expressed by spherical harmonics, which are global averages by nature;
- The results of satellite altimetry are epoch-wise, while the fields of satellite gravimetry are time averaged.

Therefore, it is impossible to deal with ocean tide aliasing in satellite gravimetry in the same way as in satellite altimetry.

Actually, the ocean tide aliasing in satellite gravimetry contains two steps. The first step is due to orbit undersampling. As a result, the ocean tides with original frequencies alias into the primary aliasing frequencies. To achieve the primary aliasing, the ocean tides are assumed to be longitudinal uniform signals, which means that the differences in amplitudes and phase lags for different longitudes at the same latitudes are ignored. These differences are taken care of in the second step. The second step is the ocean tides with primary aliasing frequencies undersampled by the gravity recovery. To be specific, if the recovery period is larger than one half of the primary aliasing period, the primary aliasing ocean tides are further undersampled and the secondary aliasing occurs. Figure 4 shows the two-step aliasing mechanism of ocean tides in satellite gravimetry.

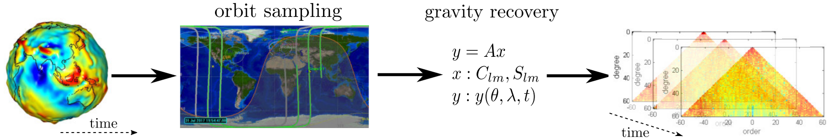

Figure 4: Two-step aliasing mechanism of ocean tides in satellite gravimetry.

Spatial downscaling of GRACE by statistical assimilation of multiple hydrological variables

GRACE has been used widely for various hydrological applications. However, the GRACE product provides the observations of the global total water storage change with coarse spatial resolution. The insufficient spatial resolution limits its application to global and large-scale studies only. Improving the spatial resolution is vital for closing the terrestrial water cycle at small scales, monitoring droughts and floods, and assessing the regional water resources.

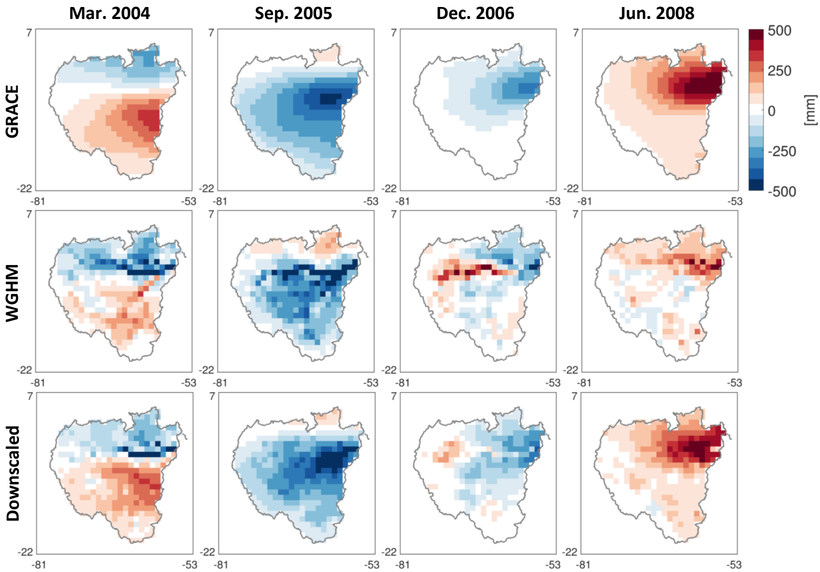

Figure 5: The total water storage change in Amazon from GRACE, WGHM and the downscaled product, at epoch Mar. 2004, Sep. 2005, Dec. 2006, Jun. 2008, respectively.

In this study, a statistical assimilation algorithm is developed for spatial downscaling of GRACE, based on a combination of moving average and partial least-squares regression. We assimilate GRACE with WGHM and multiple hydrological variables (i.e. precipitation, evapotranspiration and runoff) from highly-resolved hydrological models. From Figure 5, a finer spatial resolution of terrestrial water storage in the Amazon basin is achieved, comparing with GRACE. For a validation, we aggregate the TWS grids within the Amazon basin. As shown in Figure 6(a), our downscaled TWS fits extremely well with GRACE, satisfying the mass conservation in a basin. Meanwhile, the downscaled TWS is capable to capture the anomalous changes that are unobservable in GRACE, at certain epochs, e.g. March 2004,

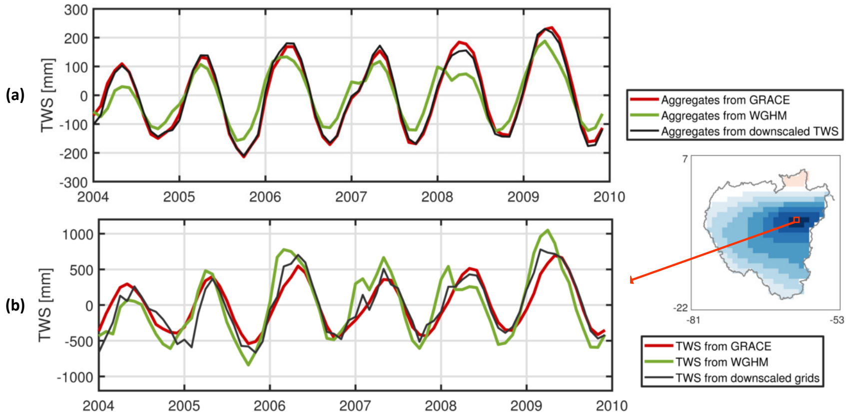

Figure 6: (a) Monthly aggregates of TWS over the Amazon basin from GRACE, WGHM and downscaled product. (b) Monthly TWS of one arbitrary grid point in the Amazon basin from GRACE, WGHM and downscaled product.

September 2005, December 2012 and June 2008, as plotted in Figure 6(b). As a result, the anomalous variations are spatially reflected in the downscaled TWS product.

In summary, the downscaled terrestrial water storage retains the dominant signals from GRACE and benefits from WGHM in local details. Our assimilation results maintain the same accuracy level of GRACE and meanwhile enhance the variation along the main river stem in the basin.

Segmentation of laser point clouds in urban areas

Segmentation denotes the task of partitioning a set (e.g. the pixels of an image or the points of a laser point cloud) into disjoint sets, whose elements share certain properties or exhibit common similarities with respect to certain attributes. In the case of images, mostly low-level features like intensity, hue or vicinity are employed as segmentation criteria; for laser point clouds also geometric attributes like local plane parameters, point densities etc. come into consideration. In the ideal case, the resulting segments form objects which are also semantically significant. In this research mobile laser data of urban areas are segmented for the purpose of building modelling and city inventory. Therefore, focus is on polyhedral objects with planar surfaces, while vegetation, vehicles, humans or curved surfaces are not subject of the investigation.

A first category of segmentation methods is based on similarity. Starting with elements having locally extremal values of a certain criterion, elements with similar values are successively aggregated by a region growing. A second category of methods is based on discontinuity. Abrupt changes in the criterion function are detected, often by evaluating gradients, in order to determine the borders between two adjacent subsets. It is advisable to determine closed borders from the very beginning, e.g. by global minimization of energy functionals.

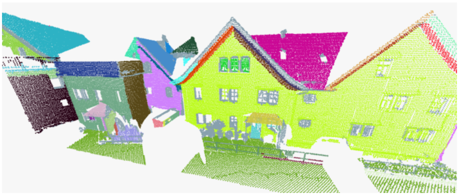

Figure 7: Details of sg_27_10 (ETH Zürich), automatic segmentation. Segments indicated by color.

In this research, the latter subdividing methods, in particular graph cut methods are employed for the segmentations. In this case the energy functional is discrete from the very beginning. The image pixels/laser points are considered as nodes of a graph, whose edges are equipped with a measure describing the similarity of the two elements. In order to find an optimal decomposition of the graph, a global loss functional is minimized, which consists in a combination of the similarity measures of the cut and possibly non-cut edges. A well-established graph-cut method is the Normalized Cut algorithm. Due to its target function, however, Normalized Cut favors cuts with short cut lines or small cut surfaces, which is a drawback for the mentioned application. Therefore in this research the target function was modified, weighting the similarity measures with distance-dependent weights. The new target function can be interpreted as a weighted average of the Cut (target functional) along the proposed border surfaces. It could be demonstrated that the minimization of this target function leads to a generalized eigenvalue problem, which can be solved with only slightly higher numerical effort compared to the Normalized Cut algorithm. An efficient method for the numerical solution of the eigenvalue problem could be pointed out, which is based on a Krylov subspace method. The algorithm can be beneficially combined with an aggregation in order to reduce the computational effort and to avoid shortcomings due to insufficient plane parameters.

The Figures 7 show details from the automatic segmentation of a well-known benchmark dataset, see `https://www.ethz.ch/content/dam/ethz/special-interest/baug/igp/photogrammetry-remote-sensing-dam/documents/pdf/Papers/timo-etal-pers2017.pdf`. The segment affiliation of the laser points is indicated by their coloring.

Estimating river depth from SWOT-type observables obtained by satellite altimetry and imagery

The Surface Water and Ocean Topography (SWOT) mission, the future hydrology and oceanography mission, will be launched in 2021. This mission aims to provide a better understanding of the world's oceans and terrestrial surface waters. It also provides an opportunity to estimate river discharge through its simultaneous measurements of water surface elevation, river width and slope. However SWOT will not observe river depth, which limits its value in estimating river discharge especially for those rivers with heterogeneous channel geometry. We aim to estimate river depth from spaceborne observations together with in situ data of river discharge. Therefore, we generate SWOT-like observables from current satellite techniques over the Po River (Figure 8) and investigate the possibility of river depth estimation from space.

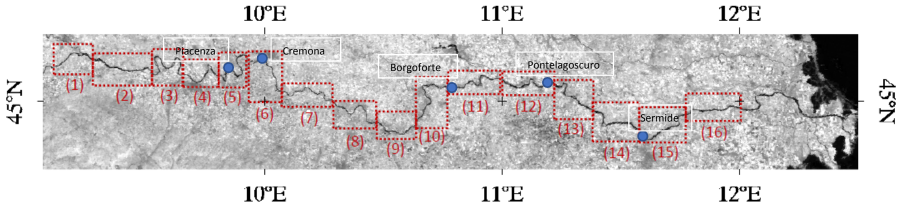

Figure 8: A MODIS image of the Po River with the selected river reaches. Blue dots are in situ stations (Tourian et al., (2017)[1]).

We obtain river water level (H) and slope (S) time series from multi-mission altimetry and effective river width (W) from satellite imagery (MODIS). Figure 9 presents an example of river water height and width time series for the reach 12. In order to estimate riverbed height, we rely on two river discharge estimation models based on the Manning equation:

$$Q = aW^{1.02}(H - H_0)^{1.74}S^{0.35} \qquad \text{developed by Bjerklie et al.}$$

$$Q = aW^{1.17}(H - H_0)^{1.57}S^{0.34} \qquad \text{developed by Dingman and Sharma}$$

Since in situ discharge measurements are available at the five stations along the river, the average riverbed's height, H_0, and the inverse of Manning's roughness coefficient, a, are the only unknown parameters in the mentioned equations. For each river reach, the discharge observations at the nearest in situ station are selected. We employ a Gauss-Helmert adjustment model to estimate H_0 and a for 16 defined reaches along the Po River.

The average river depth estimates along the Po River are validated against surveyed cross-section information (Figure 10(left)). For each reach, we obtained five estimates of H_0, for

[1] Tourian, M.J., O. Elmi, A. Mohammadnejad, and N. Sneeuw: Estimating River Depth from SWOT-Type Observables Obtained by Satellite Altimetry and Imagery, Water 9, no. 10: 753

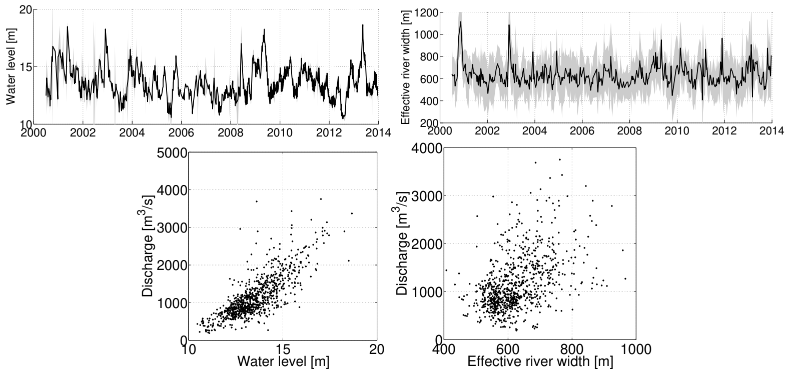

Figure 9: (top panel) Water level time series from satellite altimetry and river width from satellite imagery for reach 12. (bottom panel) Scatter plot of river discharge against water level and river width.

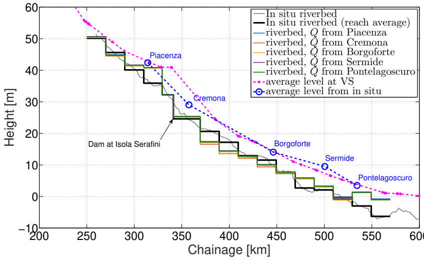

Reach	H_0^{ins} (m)	Model by Bjerklie et al.			Model by Dingman and Sharma		
		$\hat{a}$	$\widehat{H_0}$(m)	$\widehat{H_0} - H_0^{ins}$ (m)	$\hat{a}$	$\widehat{H_0}$ (m)	$\widehat{H_0} - H_0^{ins}$ (m)
1	50.27	0.69	50.37 ± 0.15	0.10	0.39	50.66 ± 0.14	0.39
2	45.62	0.60	44.72 ± 0.15	0.89	0.30	44.96 ± 0.14	0.66
3	40.09	1.36	41.47 ± 0.10	1.38	0.67	41.69 ± 0.09	1.59
4	35.91	2.06	40.73 ± 0.03	4.83	0.88	40.85 ± 0.03	4.94
5	32.20	29.20	32.07 ± 0.01	0.12	11.95	32.13 ± 0.01	0.07
6	24.60	0.80	24.91 ± 0.09	0.31	0.40	25.16 ± 0.08	0.57
7	20.63	0.22	16.06 ± 0.31	4.56	0.13	16.53 ± 0.31	4.10
8	17.18	0.27	13.06 ± 0.26	4.12	0.16	13.58 ± 0.26	3.60
9	12.92	0.74	12.07 ± 0.14	0.85	0.42	12.48 ± 0.13	0.44
10	11.54	0.50	9.37 ± 0.16	2.17	0.27	9.77 ± 0.16	1.77
11	7.38	0.53	7.04 ± 0.16	0.34	0.29	7.48 ± 0.16	0.10
12	2.70	1.40	5.64 ± 0.07	2.94	0.73	5.91 ± 0.07	3.21
13	2.08	1.25	3.00 ± 0.10	0.92	0.66	3.31 ± 0.09	1.23
14	−0.26	0.58	-1.49 ± 0.20	1.23	0.34	-0.87 ± 0.19	0.61
15	−3.00	4.83	1.07 ± 0.04	4.07	2.28	1.23 ± 0.04	4.24
16	−6.29	4.97	-1.32 ± 0.08	4.97	2.64	-1.07 ± 0.07	5.22

Figure 10: (left) Estimated riverbed profile along the Po River for 16 defined reaches. (right) Comparison between estimated and measured river bed height H_0 using the two selected models (Tourian et al., (2017)).

which we use different discharge data. Interestingly the estimated H_0 for each reach is nearly independent of the choice of discharge data. The comparison between estimated and surveyed (black steps) H_0 shows a general good agreement between the measured and estimated average riverbed profiles. The results in the table also show that both models can estimate the riverbed height with the accuracy in the range of $10\,\%$ relative root mean squared error.

The SWOT mission will provide a comprehensive view of the spatial and temporal dynamic of inland water bodies from space. Scientists will use its simultaneous surface water height, area and slope (for river reaches) measurements for calculating water volume variations in lakes, reservoirs and wetlands as well as estimating river discharge. In this study we present another perspective of the SWOT mission by estimating the average riverbed height.

Waveform retracking by using neural networks

Satellite altimetry is now a standard tool to measure the surface height of inland water bodies. However, originally satellite altimetry missions were designed to measure ocean water heights. To do so, short radar signals are transmitted in nadir direction towards the Earth. The signal, which is reflected by the surface, is then examined by the on-board instruments. Thereby, the time which the signal needs for its round trip is equal to the distance of the satellite to the Earth surface. Thus, the reflected signal is used to create a so called waveform, which contains the reflected signals and is then used to analyse the satellite height over the surface. Examples of these waveforms can be seen in Figure 11. Because the water is reflecting very strong, the waveforms caused by reflections over the ocean surface show a distinct pattern, so that the height can be estimated without problems. However, by measurements over inland water areas the radar altimeter faces more difficulties. The reason is, that the transmitted signal is now not only reflected by the inland water body, but also by the surrounding landscape. This leads to noisy peaks inside the waveforms and therefore the distance between the satellite and the Earth surface can not be estimated properly. Typically, the satellite altimeter estimates the strong water peak and fixes it at a distinct position inside the waveform. However, in waveforms over inland water areas this position is missed and one needs to apply special algorithms to find it. These algorithms are called retracker, which can estimate the peaks, caused by the strong reflection of the radar signal on water surfaces inside the waveforms.

In this study, we propose a new retracker, tackling the problem as a classification problem. We define different labels for each part of the waveform either as noise or as signal. This will be done by using a so called artificial neural network, which can be trained with very different sets of data and learns how to recognize the searched pattern. To demonstrate now the possibilities of the neural network, we apply it on the Cupari river, which is located inside the Amazon river basin in Brazil by using data of the Jason-2 satellite. (Figure 11).

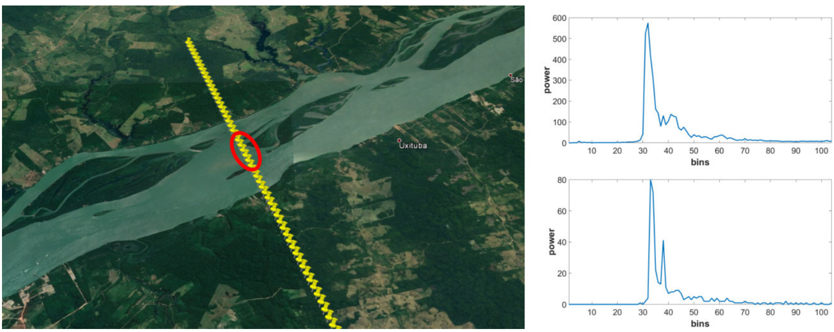

Figure 11: The Cupari river with the used track and in red, the virtual station is marked, as well as two waveform examples which were measured over the river

At first, we define a virtual station at the center of the river, in which we assume that the whole area has the same height. The data has then to be separated in training, validation and test data sets. After labeling the waveform elements and normalization the training and validation data can be applied to the neural network. In this study we decided to use a single layer feed forward neural network. Thus, only one hidden layer is used and the signal is going strictly from the input layer towards the output layer (Figure 12). During this process, the neural network adjusts its parameters so that it is able to distinguish the two labels and to recognize the characteristic pattern in new data sets. In a last step, the test data can be applied, which contains data we want to analyse. To see the performance of the neural network, we compare it with the in situ data as well as the water height, which is derived by the MLE3 retracker, the on-board retracker of the Jason-2 satellite. The resulting time series can be seen in Figure 13. This shows, that the neural network performs at least comparable with the MLE3 retracker. However, it also shows in some parts even better results. This can also be seen through the standard deviation of the residuals. Whereas the MLE3 retracker reaches an RMS of 1.241 m, the neural network approach has 1.147 m, which is nearly one decimetre improvement.

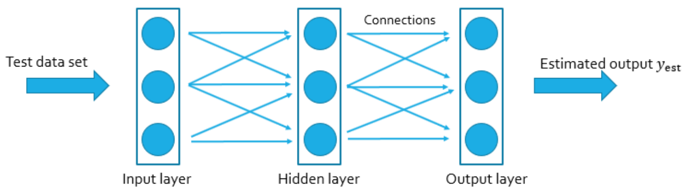

Figure 12: Sketch of a single layer feed forward neural network.

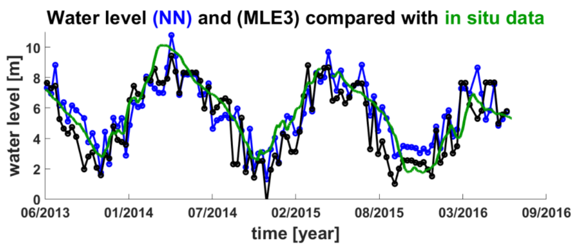

Figure 13: Comparison of the neural network (NN) and the MLE3 time series with in situ data.

This first test already showed the possibilities which are offered by the usage of neural networks. Future studies could involve other neural networks like

- Recurrent neural networks (RNN)
- Extreme learning machines (ELM)

Estimation of river discharge and surface water storage from space-borne data: full catchment coverage with optimal space and time resolution

Interest in the global freshwater system has been increasing during the last decades, with respect to its role in the Earth system and the sustainable development of water resources. On the one hand, water transport and storage on continents play an important role for atmospheric processes (climate feedback), variability of global and regional sea levels, and global biogeochemical cycles, and have a significant impact on temporal variations of the Earth's gravity field, deformation of the Earth's crust, and Earth rotation in space.

Measurement of river streamflow and water storage variation are vital for such investigations as it gives a reliable estimate of freshwater fluxes over the continents. Despite such importance, the number of river discharge gauging station has been decreasing. At the same time, information on the global freshwater system has been increasing because of various types of ground observations, water-use information and spaceborne geodetic observations. Nevertheless, we cannot answer properly crucial questions about the amount of freshwater available on a certain river basin, or the spatial and temporal dynamics of freshwater variations and discharge, or the distribution of world's freshwater resources in the future.

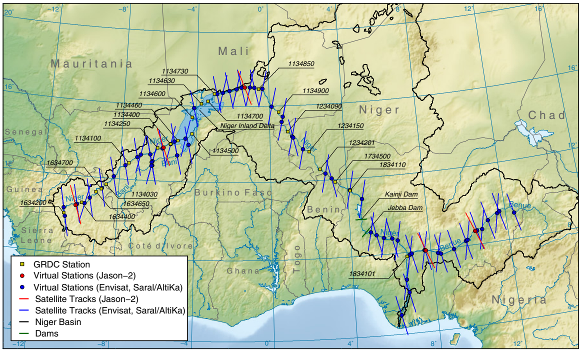

Figure 14: Available in situ discharge stations (yellow squares) and altimetric virtual stations (blue and red dots) from different missions over the Niger River. Our aim is to go beyond the conventional single-reach approach for estimating discharge and estimate daily river discharge at any given location along the river system (Tourian et al., (2017)[2]).

Insufficient observational evidence of hydrological parameters at the global scale is a major impediment for progress in hydrological modeling. Although spaceborne sensors offer a

[2]Tourian, M.J., C. Schwatke, and N. Sneeuw: River discharge estimation at daily resolution from satellite altimetry over an entire river basin, Journal of Hydrology, 546: 230-247, doi: 10.1016/j.jhydrol.2017.01.009

synoptic and global view by their very nature, satellite products do have their own limitations in terms of accuracy, temporal resolution and spatial coverage. Figure 14 presents in situ stations and virtual stations from different satellite altimetry missions along the Niger River. This example shows how available measurements are spatially and temporally sparse.

This project aims to greatly improve the observational database for two key hydrological variables, river discharge and surface water storage, by innovative modeling of results from satellite altimetry (water level) and satellite imagery (surface area). The following objectives will be addressed within this project:

- modifying the existing single-stem densification of altimetric measurements for applying on the entire river basin.
- improving the river discharge estimation algorithms from multi-mission altimetry over full catchments.
- quantifying the amount of surface water storage change within total storage variations

Assessment of radar altimetry-based river water level time series densification methods

River water level time series at geographical locations visited by satellite altimetry missions, so called virtual stations, have been produced from single altimeter river crossings already for many years. The problem is that the temporal resolution achieved in such time series is limited to the repeat cycle of the chosen altimetry mission, i.e., 10–35 days. This is insufficient for many hydrological applications where at least a 1–2 day-sampling resolution is ideally required. At the same time, the number of in-situ river gauging stations has been in a rapid decline in the past decade or so. This has been either due to a lack of proper maintenance of such stations so that they have gone out of order or due to a changes in data distribution policies of countries in charge of those stations. Either way, the remaining stations are distributed too poorly to be relied upon for a sufficiently comprehensive monitoring of water level variations along a river. Consequently, satellite altimetry technique remains today the primary source of information about water height variations along rivers. However, as mentioned above, data collected by this technique form a single altimeter are constrained in time to repeat cycle of the satellite and in space to distribution of its virtual stations. Nevertheless, a combination of measurements acquired by all available altimetry missions, repeat and non-repeat ones, along a river at their various virtual stations may allow for producing water level time series along the river with an improved temporal and spatial resolution. To that end, two methods have been developed so far: (i) Tourian et al. (2016)[3] at the Institute of Geodesy at University of Stuttgart; and (ii) Boergens et al. (2017)[4] at DGFI (Deutsches Geodätisches

[3] Tourian MJ, Tarpanelli A, Elmi O, Qin T, Brocca L, Moramarco T, Sneeuw N (2016) Spatiotemporal densification of river water level time series by multimission satellite altimetry, Water Resour Res, 52, doi: 10.1002/2015WR017654.

[4] Boergens E, Buhl S, Dettmering D, Klüppelberg C, Seitz F (2017) Combination of multi-mission altimetry data along the Mekong River with spatio-temporal kriging, J Geod, 91: 519 – 534, doi: 10.1007/s00190-016-0980-z.

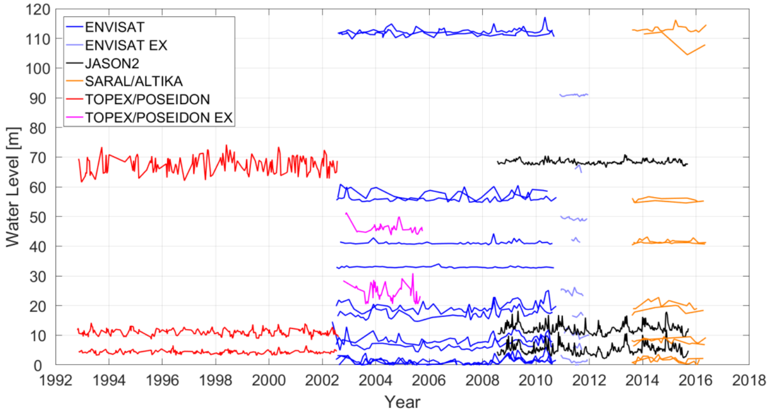

Figure 15: Water level time series collected by various satellite altimetry mission, considered in this contribution, at all virtual stations along the Po river in the time interval 1992–2018.

Forschungsinstitut) at Technical University of Munich. The former is based on a combination of hydraulics and statistics, whereas the latter is primarily a statistical interpolation scheme, so-called a kriging interpolation. The core part of the hydraulic statistic densification method is to estimate the river flow velocity model. Consequently, the time lags between virtual stations along the river can be estimated and in this way all virtual stations can be connected with each other. Differently, the kriging densification method centres around the kriging interpolation and modelling of spatial and temporal empirical covariance functions to acquire the weights among different observations. Unfortunately, the corresponding studies have been numerically conducted under different conditions. For instance, different rivers were chosen and different combinations of altimetry missions were exploited. Radar altimetry measurements used in those two studies were subject to different processing techniques, too. Such differences make a comparison between these two approaches difficult and open to interpretations. This triggered a research at the Institute of Geodesy to implement these two methods and compare them numerically under the same set of circumstances. That is, in this contribution, the same river and the same combination of radar altimetry missions were chosen. The same processing technique was applied to altimetry measurements. The combination was conducted for the same set of virtual stations. And, last but not least, the same in situ control data were exploited for validation. The outcome of such an investigation is a valuable addition in the sense that it would allow to determine which method to be chosen for future attempts in densifying river water level time series from altimetry missions. The Po river in the Northern Italy was chosen as a first attempt to perform such an assessment.

Figure 15 shows water level time series for different altimetry missions exploited in this study at all virtual stations along the chosen river in the time interval 1992–2018. The picture

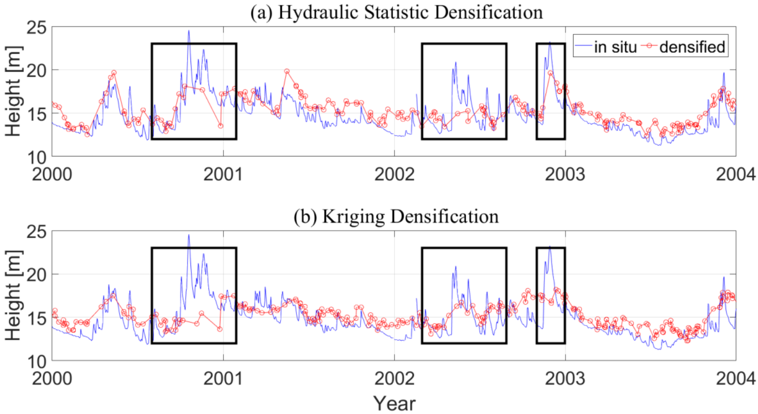

Figure 16: Water level time series densified with (a) the hydraulics statistic and (b) kriging methods versus in-situ control data at one gauging station.

additionally lists the satellite altimetry missions used in this comparison. Figure 16 compares altimetry-derived time series densified by the two aforementioned methods with in-situ data at one gauging control station along the river.

Results indicate that the two densification methods are in general comparable with each other. They reveal some differences, which are highlighted in some boxes marked in Figure 16. It is worth mentioning that the hydraulic statistic densification method still has a potential for further improvements. This lies in the fact that this method is heavily dependent on the river velocity model. The flow velocity models that we used in this contribution were not flawless and could be substantially improved for a future work. Furthermore, it is planned to repeat this comparison in a different river that has been relatively less affected by human interventions and constructions. A potential candidate for such a follow-on research is the Mekong river in Vietnam, which was used by Boergens et al. (2017), too.

Monitoring the restoration endeavors of imperiled Lake Urmia using spaceborne observations

Lake Urmia, once the largest permanent hypersaline lake in the world, has been shrinking at an alarming rate during the last two decades. Unsustainable water management in confronting with increasing demand and climatic extremes have given rise to the observed depletion of the lake. The desiccation of Urmia Lake has raised national and international concern. Based on research findings, short and long-term approaches have been proposed to revive the lake suffering from water bankruptcy. Revising the surface water management, improving the efficiency of the irrigation systems, introducing water market, increasing public awareness to conserve water and averting new dam construction are the main strategies that have been advocated. The government of Iran has established the Urmia Lake Restoration Program, ULRP, a ten-year program (2015–2025) to save Lake Urmia. It includes three phases: i) stabilizing the current status; ii) restoration; and iii) sustaining the restoration. Although many papers have addressed the causes of the desiccation, a comprehensive assessment of the state of the Urmia Lake after starting the restoration program is missing.

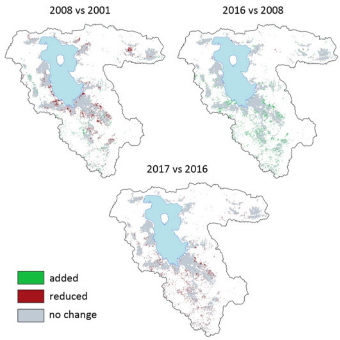

Figure 17: Agricultural area change during certain time periods using MODIS satellite land cover product.

To fill this void, we employed space-borne observations to monitor the lake and its basin mainly during the last five years of restoration endeavors. We monitor the surface water extent using satellite imagery and the lake water level using satellite altimetry (Figure 18A and B). The combination of these two parameters with the bathymetry of the lake gives us the water volume of the lake (Figure 18C). Moreover, precipitation and evaporation over the lake and its basin are monitored, especially over the last five years. The water storage change of the Urmia Lake catchment is monitored using the Gravity Recovery and Climate Experiment (GRACE) satellite observations, which enable monitoring of deep water change (Figure 18D). Expansion of irrigated area is reported as a main cause of desiccation. Hence, the agricultural land area is monitored over the last two decades using the result from MODIS satellite (Figure 17). We employed complementary data available for the Urmia basin and the lake including in situ data of the inflow to the lake, and in situ groundwater data. Observations indicate stabilization of Lake Urmia over the past three years, which release of water behind the dams played the major role. This big contribution from dams rise concern about the sustainability of the stabilization. The outcome of the study helps us evaluate the effectiveness of the recent years proceedings to some extent. Moreover, it supports future water resources management decisions and operations in the basin.

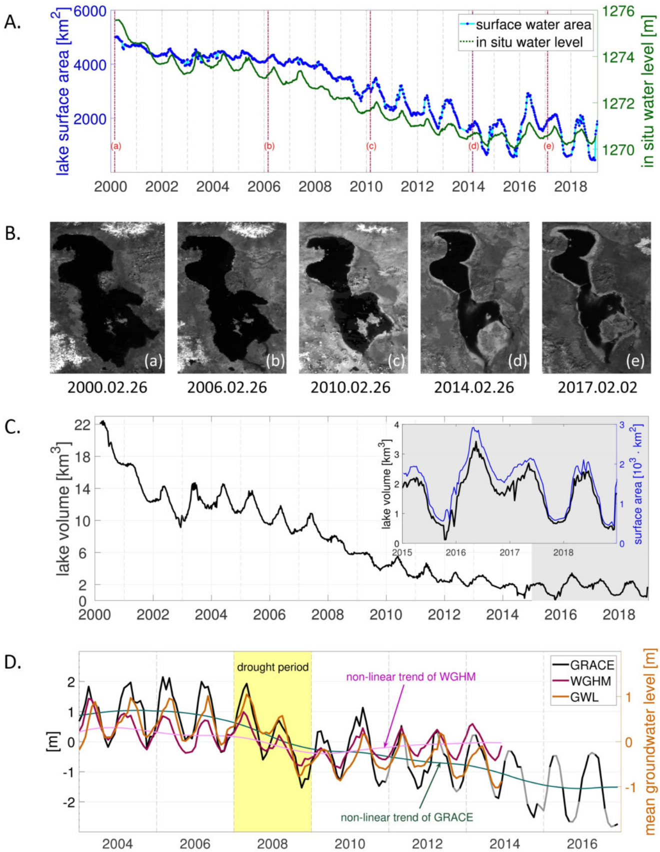

Figure 18: The result from employing space-borne observations; A) Time series of surface water extent obtained from MODIS imagery accompany with the time series of in situ water level; B) Screen shots of the lake for some dates of the surface water extent time series; C) Time series of lake water volume; D) Total water storage change time series over the Urmia catchment using GRACE compared with a WaterGAP model and piezometric wells water level.

Publications

(https://www.gis.uni-stuttgart.de/en/research/publications/index.html)

Refereed Journal Publications

Dutta, A., J. Engels, and M. Hahn (2018): Segmentation of Laser Point Clouds in Urban Areas by a Modified Normalized Cut Method. In: IEEE Transactions on Pattern Analysis & Machine Intelligence. issn: 0162-8828. doi: 10.1109/TPAMI.2018.2869744.

Lin, Y., J. Yu, J. Cai, N. Sneeuw, and F. Li (2018): Spatio-Temporal Analysis of Wetland Changes Using a Kernel Extreme Learning Machine Approach. In: Remote Sensing 10.7, p. 1129. doi: 10.3390/rs10071129.

Mink, R., A. Dutta, G. G. Peteinatos, M. Sökefeld, J. J. Engels, M. Hahn, and R. Gerhards (2018): Multi-Temporal Site-Specific Weed Control of Cirsium arvense (L.) Scop. and Rumex crispus L. in Maize and Sugar Beet Using Unmanned Aerial Vehicle Based Mapping. In: Agriculture 8.5, pp. 1–14.

Schlesinger, R. and M. Cieslack (2018): Simultane Messungen mit zehn Scintrex-CG-5-Gravimetern im stationären Parallelbetrieb. In: avn 125.8-9, pp. 274–283.

Shepherd, A. and IMBIE-team (2018): Mass balance of the Antarctic Ice Sheet from 1992 to 2017. In: Nature 558.7709, pp. 219–222. doi: 10.1038/s41586-018-0179-y.

Tarpanelli, A., E. Santi, M. J. Tourian, P. Filippucci, G. Amarnath, and L. Brocca (2018): Daily River Discharge Estimates by Merging Satellite Optical Sensors and Radar Altimetry Through Artificial Neural Network. In: IEEE Transactions on Geoscience and Remote Sensing, pp. 1–13. doi: 10.1109/TGRS.2018.2854625.

Tourian, M., J. Reager, and N. Sneeuw (2018): The Total Drainable Water Storage of the Amazon River Basin: A First Estimate Using GRACE. In: Water Resources Research 54.5, pp. 3290–3312. doi: 10.1029/2017wr021674.

Varga, P., E. Grafarend, and J. Engels (2018): Relation of Different Type Love–Shida Numbers Determined with the Use of Time-Varying Incremental Gravitational Potential. In: Pure and Applied Geophysics 175.5, pp. 1643–1648. doi: 10.1007/s00024-017-1532-z.

Vishwakarma, B., B. Devaraju, and N. Sneeuw (2018a): What is the Spatial Resolution of GRACE Satellite Products for Hydrology? In: Remote Sensing 10.852, 17 pages. doi: 10.3390/rs10000852.

Ye, Z., R. Tenzer, and N. Sneeuw (2018): Comparison of methods for a 3-D density inversion from airborne gravity gradiometry. In: Studia Geophysica et Geodaetica 62.1, pp. 1–16. doi: 10.1007/s11200-016-0492-6.

Yuan, P., W. Jiang, K. Wang, and N. Sneeuw (2018): Effects of Spatiotemporal Filtering on the Periodic Signals and Noise in the GPS Position Time Series of the Crustal Movement Observation Network of China. In: Remote Sensing 10.9, p. 1472. doi: 10.3390/rs10091472.

Books & Miscellaneous

Antoni, M. (2019): Calculus with Curvilinear Coordinates — Problems and Solutions. Springer International Publishing. isbn: 978-3-030-00415-6. doi: 10.1007/978-3-030-00416-3.

Grafarend, E. (2018b): "The Global World of A. Dermanis and an attempt to use System Dynamics for the analysis of Polar-Motion (PDM) and Length of Day Variations (LOD)". In: Quod Erat Demonstrandum - In quest of the ultimate geodetic insight, Special issue for Professor Emeritus Athanasios Dermanis. School of Rural and Surveying Engineering, AUTH 2018, pp. 1–36.

Conference Presentations

Cai, J., D. Dong, N. Sneeuw, and Y. Yao (2018): Converted total least squares method and Gauss-Helmert model with applications in coordinate transformations. Hotine-Marussi Symposium, Rome, 18–22 June.

Grafarend, E. (2018a): Geodesy: The Challenge of the Third Millenium. General Assembly of the Nordic Geodetic Commission (NGC) Helsinki, Finland (22.8–10.9).

Liu, W. and N. Sneeuw (2018): A triple-pair tandem constellation mitigating ocean tide aliasing. International Symposium Gravity, Geoid and Height Systems 2, Copenhagen, Denmark, Sep 17–21.

Purkhauser, A., R. Pail, M. Hauk, P. Visser, N. Sneeuw, P. Saemian, W. Liu, J. Engels, Q. Chen, C. Siemes, et al.: Gravity Field Retrieval of Next Generation Gravity Missions regarding Geophysical Services: Results of the ESA-ADDCON Project. EGU General Assembly, Wien, 8–13 April.

Sjöberg, L., E. Grafarend, and M. Joud (2018): Zero gravity curve and surface. Hotine-Marussi Symposium 2018, Rome, 18–22 June.

Sneeuw, N., M. Tourian, and J. Reager (2018): Can GRACE observe the total drainable water storage of a river basin? A first estimate over the Amazon basin. Hotine-Marussi Symposium, Rome, 18–22 June.

Sneeuw, N. (2018): Spaceborne Gravimetry: Technology, Missions and Applications. International Top-level Forum on Engineering Science and Technology Development Strategy, Chinese Academy of Engineering, Wuhan, China.

Sneeuw, N., J. T. Reager, and M. Tourian (2018): Total drainable water storage from space-borne gravimetry. Chinese Academy of Surveying and Mapping, Beijing, PR China.

Vishwakarma, B., B. Devaraju, and N. Sneeuw (2018b): What is the spatial resolution of GRACE satellite products for hydrology? Hotine-Marussi Symposium 2018, Rome, 18–22 June.

Yin, Z. and N. Sneeuw (2018): Modelling the gravitational field by using CFD techniques. Hotine-Marussi Symposium, Rome, 18–22 June.

Poster Presentations

Behnia, S., T. Wang, and N. Sneeuw (2018): What can we learn from satellite altimetry over salt flats? A case study using CryoSat-2 over Salar de Uyuni. 25 Years of Progress in Radar Altimetry Symposium, Ponta Delgada, Portugal.

Douch, K., A. Knabe, H. Wu, J. Müller, and G. Heinzel (2018): What is Required to Recover the Time-variable Gravitational Field Using Satellite Gradiometry? Gravity, Geoid and Height Systems, Copenhagen, Denmark.

Iran-Pour, S., M. Weigelt, A. Amiri-Simkooei, and N. Sneeuw (2018): Orbit optimization for future gravity field missions: the influence of the choice of time variable gravity field models. Hotine-Marussi Symposium, Rome, 18–22 June.

Master Theses

(`http://www.gis.uni-stuttgart.de/en/theaching/theses/`)

Balangé, Laura: Implementierung der Meeresspiegelgleichung.

Li, Yang: Complex Singular Spectrum Analysis of Earth Orientation Time Series

Qian, Kun: The Optimal Regularization and its Application in Extreme Learning Machine for Regression Analysis and Multi-class Classification

Xia, Ruiheng: Characterization of runoff-storage relationships in boreal catchments

Xia, Zhuge: Assessment of Radar Altimetry River Water Level Data Densification Methods

Zhao, Daixin: Generating water level time series from satellite altimetry measurements for inland applications

Bachelor Theses

Li, Fanxiang: Sea Surface Altimetry using GNSS–R

Liu, Mo: Analyzing the Surface Height of Nam Co by using CryoTrack

Ouyang, Jiamin: The effect of solar radiation pressure on the Sun-synchronous satellite GOCE

Yan, Lun: Water level analysis in Tibet using CryoSat-2

Guest Lectures and Lectures on special occasions

Fukushima, T (National Astronomical Observatory of Japan): New numerical approach to compute gravitational field of general object accurately (Colloqium at Institute of Geodesy, University of Stuttgart, 6.9)

Keller, W (Institute of Geodesy, University of Stuttgart): Wie viel Mathe braucht der Geodät? (Geodätisches Kolloqium, 9.11)

Künzer, C (Deutsches Zentrum für Luft- und Raumfahrt):Die Dynamik der Landoberfläche – Potentiale und Herausforderungen der Fernerkundung (Geodätisches Kolloqium, 2.2)

Sneeuw, N (Institute of Geodesy, University of Stuttgart): Rosborough representation in satellite gravimetry (Colloqium at Institute of Geodesy, University of Stuttgart, 6.9)

Yamamoto, K (National Astronomical Observatory of Japan): Introduction of image landmarks to spacecraft orbit determination (15.3)

Yin, Z (School of Geodesy and Geomatics, Wuhan University, China): Modelling the gravitational field by using Computational Fluid Dynamics (CFD) techniques (Colloqium at Institute of Geodesy, University of Stuttgart, 6.9)

Lectures at other universities

Grafarend E: Geodesy – the Challenge of the Third Millenium, Technical University of Budapest, Budapest, Hungary (21.9)

Grafarend E: Geodesy – the Challenge of the Third Millenium, Research Institute for Geodesy and Geophysics, Sopron, Hungary (24.9)

Sneeuw N: Hydro-Geodesy: geodetic satellite methods for hydrological purposes, TU Delft, Delft, The Netherlands (27.2)

Sneeuw N: Total drainable water storage from spaceborne gravimetry, Chinese Academy of Surveying and Mapping (CASM), Beijing, China (11.–18.5)

Activities in National and International Organizations

Grafarend E.

Professor h.c., University of Navarra, Pamplona, Spain
Professor h.c., University of Tehran, Iran
Professor h.c., Wuhan University, China
Fellow International Association of Geodesy (IAG)
Elected Member of the Finnish Academy of Sciences and Letters, Finland
Elected Member of the Hungarian Academy of Sciences, Hungary
Member Royal Astronomical Society, Great Britain
Corresponding Member Österreichische Geodätische Kommission (ÖGK)
Emeritus Member German Geodetic Commission (DGK)
Gauss Society, Göttingen
Member of the "Leibniz Gesellschaft der Wissenschaften", Berlin
Member Flat Earth Society
Elected Member Leibniz-Sozietät, Berlin

Keller W.

Doctorate honoris causa, Wrocław University of Environmental and Life Sciences, Wrocław, Poland

Sneeuw N.

Professor h.c. (Luojia chair), Wuhan University, China
Fellow International Association of Geodesy (IAG)
Member Assessment Panel Space Research, NWO, Netherlands
Search Committee Politecnico Milano, Italy
Full Member Deutsche Geodätische Kommission (DGK)
Member of GGOS working group Committee on Satellite Missions
Member of Gauss-Gesellschaft e.V., since 2018
Member of AK7 (working group 7), Experimentelle, Angewandte und Theoretische Geodäsie, within DVW (Gesellschaft für Geodäsie, GeoInformation und LandManagement), 2015–2018
Member of the editorial board of Surveys in Geophysics
Member of the editorial board of Studia Geophysica et Geodaetica

Courses – Lecture/Lab/Seminar

Bachelor Geodesy and Geoinformatics (German):

Amtliches Vermessungswesen und Liegenschaftskataster (Grams)	2/0/0/0
Ausgleichungsrechnung I, II (Krumm, Douch, Elmi)	3/1/0/0
Einführung Geodäsie und Geoinformatik (Sneeuw)	2/2/0/0

Integriertes Praktikum/Integrated Field Work (Keller, Sneeuw)	10 days
Landesvermessung (Krumm, Antoni)	2/2/0/0
Physikalische Geodäsie (Sneeuw, Hashemi Farahani)	2/2/0/0
Referenzsysteme (Sneeuw, Douch)	2/2/0/0
Satellitengeodäsie (Sneeuw, Douch)	1/1/0/0
Wertermittlung I (Bolenz)	2/0/0/0

Master Geodesy and Geoinformatics (German):

Aktuelle Geodätische Satellitenmissionen (Sneeuw)	2/2/0/0
Amtliche Geoinformation (Heß)	2/0/0/0
Ausgewählte Kapitel der Parameterschätzung (Krumm, Engels)	2/2/0/0
Erderkundung (Sneeuw)	2//0/0/0
Geodynamische Modlle (Engels, Douch)	2/2/0/0
Grundstücksbewertung II (Bolenz)	2/0/0/0
Koordinaten- und Zeitsysteme in der Geodäsie (Sneeuw)	2/0/0/0
Physikalische Geodäsie (Engels)	2/2/0/0
Satellitengeodäsie (Sneeuw, Hashemi Farahani)	2/1/0/0

Master GeoEngine (English):

Advanced Mathematics (Antoni)	3/2/0/0
Foundations of Satellite Geodesy (Sneeuw, Hashemi Farahani)	2/1/0/0
Integriertes Praktikum/Integrated Field Work (Keller, Sneeuw)	10 days
Map Projections and Geodetic Coordinate Systems (Krumm, Antoni)	2/1/0/0
Physical Geodesy (Sneeuw, Hashemi Farahani)	2/1/0/0
Satellite Geodesy Observation Techniques (Sneeuw, Hashemi Farahani)	2/1/0/0
Statistical Inference (Krumm, Douch)	2/1/0/0

Institute of Navigation

Breitscheidstraße 2
D-70174 Stuttgart
Tel.: +49 711 685 83400
Fax: +49 711 685 82755
ins@nav.uni-stuttgart.de
http://www.nav.uni-stuttgart.de

Head of Institute

Prof. Dr.-Ing. Alfred Kleusberg (until 07/18)
Prof. Dr.techn. Thomas Hobiger (from 08/18)

Deputy: Dr.-Ing. Aloysius Wehr
Secretary: Helga Mehrbrodt

Staff

Dipl.-Ing. Doris Becker	Navigation Systems
Dipl.-Geogr. Thomas Gauger	GIS Modelling and Mapping
M.Sc. Tomke Jantje Lambertus (from 11/18)	Parameter Estimation in Dynamic Systems
Dipl.-Ing. (FH) Martin Thomas	Laser Systems, Digital Electronic and Hardware Programming
Dr.-Ing. Aloysius Wehr	Laser Systems, Optical and Wireless Communication

EDP and Networking

Regine Schlothan

E-Laboratory and Precision Mechanical Workshop (ZLW)

Dr.-Ing. Aloysius Wehr (Head of ZLW)
Sebastian Schneider (Electrician)
Michael Pfeiffer (Mechanician Master)

External teaching staff

Hon. Prof. Dr.-Ing. Hans Martin Braun - RST Raumfahrt Systemtechnik AG, St.Gallen

Preface

Driven by the appointment of Prof. Hobiger as the institute's new chair, four main research focus areas were defined, Those areas which will be assigned staff and projects in the coming years. Figure 1 depicts those areas which are all grouped around the topics of "positioning and navigation".

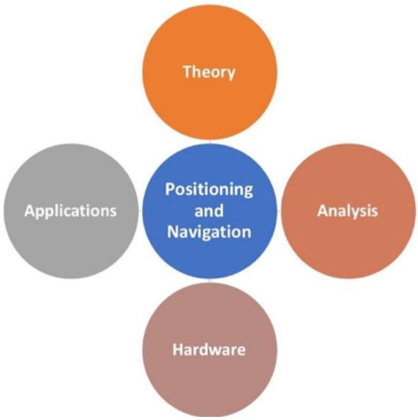

Figure 1: *The INS will focus on 4 fields of research which are grouped around the topics of "positioning and navigation".*

The research field "Theory" involves the investigation and testing of mathematical models in order to improve existing positioning methods. The adaptation of classical parameter estimation methods and the development of new mathematical algorithms are key elements for innovative navigation applications. In this context the main focus lies on the realization of real-time solutions in order to facilitate mobile navigation applications (e.g. smartphones) or commercial high-precision applications. Investigations concerning the optimal weighting of sensor data are also a field of research. In addition, non-linear systems and their peculiarities are studied as well. The research output from this topical focus is a precursor to other research topics but also benefits from feedback from application-oriented fields of research.

In order to test new algorithms and navigation solutions the institute has started to develop its own inhouse suite of software tools. The INS develops and maintains open-source solutions, offered to users after testing and validation. In addition, the exploration and testing of improved adjustment models for positioning and navigation of static and moving objects is another topic of research. These efforts are complemented by studying systematic effects, which set an implicit limit for improving the accuracy of positioning solutions. Among those effects, atmospheric delays and instrumental effects are currently under investigation. These efforts lead an overlap with the research field "Hardware" and there are clear links to aerospace applications, especially to the positioning of nanosatellites. The constantly increasing number of those satellites makes cost-effective solutions possible but requires also precise orbit determination for these extremely low-flying objects.

The third research focus involves hardware components for positioning and navigation and is based upon the institute's own infrastructure. The combination of different sensor elements is a crucial approach when designing optimal navigation solutions for certain applications. Beside various inertial navigation systems the usage of novel sensors is examined. In doing so, the overall goal to develop and test hybrid measurement systems is pursued. Together with results from fundamental research and input from industry, new measurement instruments and sensors can be tested for their positioning and navigation abilities on different platforms. Furthermore, software-based GNSS-receivers are developed in order to test new signal structures and to perform verification experiments before commercial receivers are available on the market. The use of such receivers in teaching is self-evident. It allows students who do not have a classical electrical engineering background to understand how GNSS receivers operate. Thus, during the laboratory courses students can experiment with various signal processing steps without the need to build electronic components or to adapt them to the receiver. This domain also relates to the constantly developing research field of nanosatellites. In cooperation with other institutes we will be able to supply navigation solutions in accordance to the requirements of space missions concerning all technical and operational specifications.

This forth field of research involves the determination of the parameters which were not anticipated when GNSS were designed. For example, GNSS measurements include important information concerning the atmospheric condition along the signal-path or multi-path signals might provide information about the geometrical and electro-magnetic environment. As for the latter, this has led to a new research field called GNSS reflectometry (GNSS-R). Since GNSS signals, which are reflected by water, ice or land surfaces, interact differently with the direct signals of the satellites one can deduce information about the reflecting surfaces. Geophysical features (e.g. geometric height, soil moisture, snow height) of the reflecting surfaces can be retrieved and be provided for weather forecasts or climate research. In a similar way, the determination of atmospheric parameters using GNSS has been another success story. Especially the determination of integrated water vapor from GNSS contributes to the improvement of the global and regional weather forecasts and has impact on different scientific projects.

In addition to these applications, research on time- and frequency generation and dissemination is being carried out. Time as the third component of positioning, navigation and timing (PNT) is a crucial component for many applications in science, industry and society. Considering that the next-generation of atomic clocks are several orders of magnitude more stable than current frequency standards, it is evident that the requirements on GNSS-based time and frequency transfer are going to increase. The INS has set put a special research focus on this topic as well.

Research Projects

Project - Laboratory Testbed Development for Testing OPS-SAT Optical Communication PCBs

OPS-SAT is an ESA project and is a synonym for a laboratory in low earth orbit which will test and validate new techniques in mission control and on-board systems. OPS-SAT has been developed with the objective to be very flexible, to offer high performance and safety at low cost. Therefore, it was decided to develop OPS-SAT on the standards applied and approved of the well-known cubesats. This means, the used printed circuit boards (PCBs) have very limited dimensions in size and are assembled with off-the-shelf electronic components. OPS-SAT is designed so, that it can be used as a test-bed for on-board software applications, for advanced communication protocols, for compression techniques, for the demonstration of advanced software-defined radio (SDR) concepts, for the optical communication from ground to space and for various experiments with special hardware like cameras and attitude control systems and for procedures with regard for scheduling and autonomy.

As the INS did not have access to the test environment of OPS-SAT, special test beds on basis of an ARDUINO and special test software in ARDUINO-C were realized in the year 2017. By applying these hard- and software tools it was possible to evaluate the performance of the component on the PCB and identify improvements concerning the PCBt's layout.

In the year 2018 the testbed was extended with a PPM-Transmitter-Module (PTM) for pulsed laser transmission, an optical receiver with housing and a simulator of the OPS-SAT on-board computer (OBCS). PTM, OBCS and optical receiver were built-up with ARDUINO boards using Atmega 328P microcontrollers and special purpose shields developed at INS. All required programs and libraries of the interfaces were written by the INS using the open-source Arduino integrated development environment (IDE). .

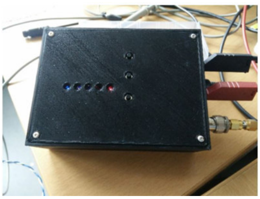

Figure 2: *PPM-Transmitter-Modul with control panel.*

The PCB of PTM is housed in a 3D printed case with an integrated control panel (Figure 2, Figure 3). The pulse rate was adapted to the maximum pulse repetition frequency (1.6 kHz) of the transmitting laser, which is located on the ground. PTM features sending either single data, a continuous data stream or data input from an USB interface. Figure 4 shows the pulse position modulation (PPM) data generator shield.

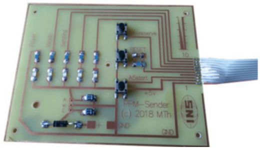

Figure 3: *Control panel PCB.*

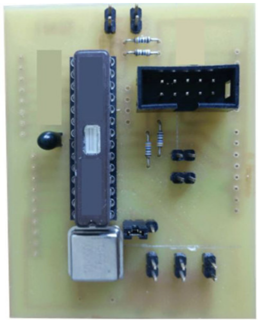

Figure 4: *Pulse position modulation (PPM) data generator shield.*

Figure 5 shows the housing of the optical receiver with the receiving optic and Figure 6 depicts the electronics. The program implemented in the Atmega 328P microcontroller assures that this item is functioning without IDE and can be controlled by OBCS. For a correct signal detection and decoding the following statuses have to be discerned: start of transmission, signal detection with Doppler correction, end of signal detection and signal outage.

OBCS controls the optical receiver on board the satellite and outputs the decoded data. The following functions and routines are implemented: control routines of the optical receiver, controlling the reference values of the receiving module, processing of the receivert's status signal, initializing, reading and deleting data stored in the on-board data memory.

Figure 5: *Optical receiver.*

Figure 6: *PCB of the optical receiver.*

Project - Modelling and Mapping Air Concentration and Atmospheric Deposition of Reactive Nitrogen Species in Baden-Württemberg for 2012 to 2016 - Preliminary Results

First preliminary results of the research project “Nitrogen background air concentration and atmospheric deposition Baden-Württemberg 2018 Part 1: Regional scale modelling”, funded by the State Agency for Environment, Baden-Württemberg (LUBW) are achieved in 2018. A project consortium is set up for carrying out the joint research, consisting of EURAD group of Rhenish Institute for Environmental Research at the University of Cologne (RIU), Interra, Kenzingen, Meteotest, Berne (CH), and INS as project leader. Within the project different modelling approaches, i.e. the chemical transport model (CTM) EURAD, the GIS based Inferential Model PolluMap, INS geostatistical models, Interra regression models, respectively, are combined in order to derive high spatial resolution maps of air concentration and atmospheric deposition of reactive nitrogen (N_r) species.

In this project the ecosystem level is represented by a 1 ha grid model output resolution for concentration and deposition fluxes of N_r species, achieved by GIS implemented modelling. Wherever possible the modelling approach makes use of measurement data, in order to avoid contradictions between reliable monitoring data and modelling results.

The Inferential Model PolluMap (Meteotest, Berne, CH) is modelling air concentration and dry deposition using 1 ha cadastral emission data, meteorological data, and very high-resolution land cover data along with CTM EURAD output data and point monitoring data of N_r on an annual base. Wet deposition, the N_r input onto exposed surfaces with precipitation, and dry deposition into forest ecosystems are calculated using GIS procedures, mainly geostatistical modelling, carried out by INS based on annual point data of monitoring together with high-resolution (1 ha) modelled fields of precipitation, and land cover data.

In Figures 7 and 8 preliminary high-resolution modelling and mapping results of ammonia (NH_3) air concentration and dry, wet and total deposition fluxes of reduced nitrogen (NH_X-N, i.e. ammonia and ammonium), including comparisons with measurement data are shown.

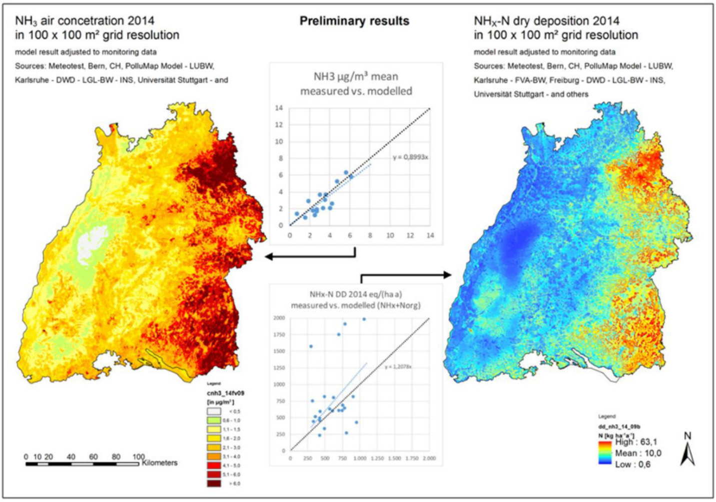

Figure 7: *Preliminary modelling and mapping results of air concentration of ammonia adjusted to measurement data and dry deposition of reduced nitrogen (NH_X-N) in Baden-Württemberg in 2014, modelled using the Inferential model PolluMap (1ha grid resolution).*

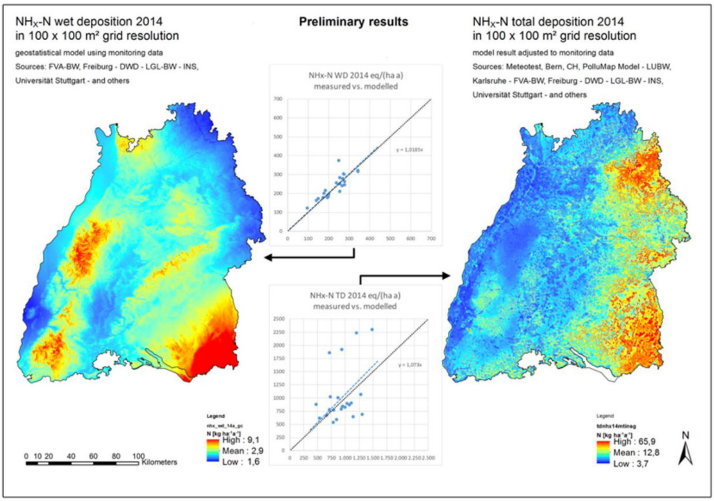

Figure 8: *Preliminary modelling and mapping results of wet and total (= wet + dry) deposition of reduced nitrogen (NH_X-N) in Baden-Württemberg in 2014 modelled using GIS application (geostatistics) and the Inferential model PolluMap. (1ha grid resolution).*

The project is part of StickstoffBW, an initiative of the federate state of Baden-Württemberg, elaborating basic information and data for regional politics and administrative execution with respect of ecological relevant nitrogen input. Project results are supporting EU and national regulations on air pollution control and emission abatement (EU NEC directive, BImSchG, TA-Luft), which are to be implemented on the sub-national level of the federate states of Germany. Moreover, scientific interest is supported by these data, e.g. for ecosystem flux assessment studies, ecological impact assessment, biodiversity, and nature protection. Administrative applications aiming at emission control and abatement of air pollutants are using the reactive nitrogen deposition data with reference to permission of projected animal husbandry, road construction, industrial settlements, and power plants, respectively. Results of the project are designated for public use and accessible via *https://www.lubw.baden-wuerttemberg.de/medienuebergreifende-umweltbeobachtung/stickstoffbw*.

Publications and Presentations

Gauger, T.: Forschungsarbeiten im Rahmen der "StickstoffBW AG1 Deposition"- Modellierung der Stickstoff Hintergrunddeposition und Konzentrationen in Baden-Württemberg 2018. 4. Sitzung des Begleit-AK "GROWA+ NRW 2021" am 13. Dezember 2018, MULNV, Düsseldorf, oral presentation, *https://www.flussgebiete.nrw.de/growa-nrw-2021-4994*.

Hobiger T. et al.: Versatile and Low-Cost GNSS-R Receivers by Means of Software Defined Radio, American Geophysical Union Fall Meeting, Washington D.C., USA, poster presentation.

Bachelor Thesis

Visualization of Parameters for the Optimum Choice of GNSS Constellations (Becker)

Master Thesis

Optimization of GNSS Positioning Concerning the Selection of Satellites, (Becker)

Attitude Determination of Data Glasses for Augmented-Reality-Visualizations in Cars (Wehr)

Evaluation of GNSS, (Becker)

SAR from Geosynchronous Orbit, (Braun)

Positioning Analysis of Different Drives With Single Frequency GNSS Receiver (Becker)

Activities in National and International Organizations

Alfred Kleusberg

Fellow of the International Association of the Geodesy
Member of the Institute of Navigation (U.S.)
Member of the Royal Institute of Navigation
Member of the German Institute of Navigation

Thomas Hobiger

AGU Geodesy Section Award 2018
Editorial board member “Journal of Geodesy”
Editorial board member “Earth, Planets and Space”
Co-chair of IAG working group 4.3.9 “GNSS-R”
Member of the Global Geodetic Observing System (GGOS) consortium
Member of the E-Infrastructure committee, Swedish Science Council
Member of the Advisory Group for Research Infrastructures, Swedish Science Council

Thomas Gauger

Member of VDI/DIN KRdL working group on Deposition parameters [NA 134-02-01-08 UA]
Member of ICP Forests
Member / Guest scientist of Bund-Länder-Fachgespäch Stickstoffdeposition (FGN)
Member of StickstoffBW, AG1 Deposition

Education (Lecture / Practice / Training / Seminar)

Introduction of Geodesy and Geoinformatic (BSc) (Hobiger, Becker)	2/2/0/0
Electronics and Electrical Engineering (Wehr)	2/1/0/0
Satellite Measurement Engineering (Wehr)	2/1/0/0
Measurement Techniques in Navigation (Wehr)	1/3/0/0
Parameter Estimation in Dynamic Systems (Hobiger, Lambertus)	2/1/0/0
Navigation I (Kleusberg)	2/2/0/0
Inertial Navigation (Hobiger, Lambertus)	2/2/0/0
Radar Measurement Methods I (Braun)	2/0/0/0
Radar Measurement Methods II (Braun)	2/1/0/0
Dynamic System Estimation (Kleusberg, Becker)	2/1/0/0
Integrated Positioning and Navigation (Kleusberg, Becker)	2/1/0/0
Satellite Navigation (Hobiger,Becker)	2/1/0/0
Interplanetary Trajectories (Becker)	1/1/0/0
Integrated Fieldwork (Becker)	(SS 2018)

Institute for Photogrammetry

Geschwister-Scholl-Str. 24D
D-70174 Stuttgart
Tel.: +49 711 685 83336
Fax: +49 711 685 83297
info@ifp.uni-stuttgart.de
http://www.ifp.uni-stuttgart.de

Head of Institute

Prof. Dr.-Ing. Uwe Sörgel

Deputy:	apl. Prof. Dr.-Ing. Norbert Haala
Personal Assistant:	Martina Kroma
Emeritus Professors:	Prof. Dr.-Ing. Dr. hc. mult. Fritz Ackermann
	Prof. Dr.-Ing. Dieter Fritsch

Academic Staff

Dipl.-Ing. Alessandro Cefalu (until 2/2018)	Photogrammetric Calibration
Dr.-Ing. Michael Cramer	Photogrammetric Systems
Dipl.-Ing.(FH) Markus Englich	Laboratory, Computing Facilities
apl. Prof. Dr.-Ing. Norbert Haala	Photogrammetric Computer Vision
M.Sc. Michael Kölle (since 11/2018)	Crowd-based Data Collection
M.Sc. Dominik Laupheimer	Classification in Remote Sensing
Dr. techn. Gottfried Mandlburger	Laser Bathymetry
M.Sc. Lavinia Runcenau (until 10/2018)	Modelling of Building Interiors
M.Sc. Stefan Schmohl	Deep Learning in 3D Remote Sensing
M.Sc. Philipp Schneider (since 10/2018)	SAR Interferometrie
Dipl.-Ing. Patrick Tutzauer	Facade Interpretation
Dr.-Ing. Volker Walter	Geoinformatics
M.Sc. Chia-Hsiang Yang (until 12/2018)	Persistant Scatterer Interferometry

Stipendiaries and external PhD Students

M.Sc. Stefan Cavegn	Image-based Mobile Mapping
M.Sc. Ke Gong	3D Reconstruction
Dipl.-Ing. Wolfgang Groß	Transformation of Hyperspectral Data
M.Sc. Rami Khamis	3D Building Modelling
Dipl.-Phys. Hendrik Schilling	Classification of Hyperspectral Data
M.Sc. Mehrdad Nekouei Sharaki	Photogrammetric Image Processing
M.Sc. Shuang Zhang	UAV Data Collection

Guests

Prof. Dr. Quanye Du	Image Orientation
M.Sc. Cesar de Paula	Laser-Bathymetrie
M.Sc. Jinghui Wang	Surface Motion Estimation

External Teaching Staff

Dipl.-Ing. Stefan Dvorak, Amt für Stadtentwicklung und Vermessung, Reutlingen

Research Activities in ifp organized in four thematic Groups

Geoinformatics	Dr.-Ing. Volker Walter
Photogrammetric Computer Vision	apl. Prof. Dr.-Ing. Norbert Haala
Photogrammetric Systems	Dr.-Ing. Michael Cramer
Remote Sensing	Prof. Dr.-Ing. Uwe Sörgel

Research Projects

Ultra-high precise and accurate UAV-based LiDAR and Dense Image Matching

One of the main research and development activities at ifp within the last year was focussing on a joined study, initiated by the German Federal Institute of Hydrology (BfG) in partnership with the Office of Development of Neckar River (ANH). This project investigates the potential of ultra-high precision UAV-based LiDAR and dense image matching. Ultra-high precision refers to the aspired 3D object point accuracy, which is in the range of a few millimetres only. So far UAV applications do not address such high accuracy. Motivation behind is the monitoring of possible subsidence for water channel infrastructures. Within the selected test site, subsidence of about 1 mm/a up to 1-3 cm/a relative to the stable surroundings has to be observed. This defines the accuracy addressed. To monitor such movements, state-of-the-art engineer-geodetic monitoring typically applies point-wise measures on the respective structures by tachymeter, precise levelling, extensometer or alignment. In contrast, we aim at area wide measurement by UAV-based monitoring using image matching and laser scanning. Hence, we are able to detect changes in areas not monitored so far, which is one of the main advantages against point-wise techniques and one of the main motivations of the whole project.

The test area is located in Hessigheim at the Neckar River, north of Stuttgart. It contains a ship lock facility, the river in the center, and the riparian area both sides of the river. The whole area size is about 570 m (east-west) x 780 m (north-south). Within 2018 two flight campaigns have been executed. One in spring (March 2018) and the second in late fall (November 2018). During these campaigns large format nadir images and dense LiDAR data were recorded from two different UAV-platforms, almost flying at the same time during the same flight day.

The photogrammetric nadir images have been captured using the CopterSystems CS-SQ8 copter that is optimized for the PhaseOne iXU RS 1000 camera payload. This camera provides 100 MPix RGB imagery with 11608 x 8708 pix each. For the March flight (as an example) 18 consecutive flight missions were necessary to fully cover the area of interest. 3775 images with nominal 80/60 overlap are arranged in 146 mostly north-south oriented flight lines, as the Neckar River's cardinal orientation is almost north-south for this test area. The mean flying height was around 40 m above ground level. This results in a nominal GSD of 3.7 mm for the nadir imagery. Each image roughly captures an area of 43 x 32 m^2 then.

The LiDAR data were captured almost in parallel with a Riegl VUX-1LR mounted on a Ri-Copter UAV platform. For the same March campaign data acquisition was carried out in 4 flight sessions comprising 17 longitudinal (i.e. north-south) strips, 4 cross strips (east-west), 4 diagonal strips to cover the steep wooded slope in the south-eastern corner of the investigation area, and two diagonal extra flight lines for further block stabilization. With a flying speed of 8 m/s, a nominal flying altitude of 50 m above ground level, a strip distance of 35 m, a pulse repetition rate of 820 kHz, a scan line rate of 133 Hz and a used scanner field-of-view of 70°, the resulting mean laser pulse density is 300-400 points/m^2 per strip and more than 800 points/m^2 for the entire flight block (i.e. nominal side overlap of 50%). This flight mission parameters guarantee a laser footprint diameter on the ground of less than 3 cm enabling a high planimetric resolution of 5 cm.

As of today LiDAR and image data have been processed separately using standard approaches. For the LiDAR the georeferencing is mainly based on the GNSS/inertial trajectory. For the refinement an additional LiDAR strip adjustment with (time dependent) trajectory correction is applied. Additional reference roof surfaces are mainly used to fix datum effects. Different versions are considered which also influence the LiDAR point cloud. Spline correction delivers smallest between-strip residuals, but introduces systematic effects in the LiDAR point cloud.

The large format PhaseOne nadir images are processed with standard bundle adjustment using additional self-calibration based on control points only. Signalized ground points are automatically extracted as they use sufficiently large checker board targets. The overall mean re-projection error is around 1/3 pix, if only the automatically measured points are considered this error improves up to 0.06 pix. Dense point clouds derived from dense image matching are processed and compared to the LiDAR point cloud.

The Figure 1 shows the comparison of the two different surface models from dense image matching (left) and LiDAR (middle). An additional profile cut (right) shows the points from the photogrammetric point cloud (red) and LiDAR points (blue). Obviously, both approaches provide a dense and accurate representation of the respective surface geometry. However, as it is also visible in the profiles from the photogrammetric and LiDAR point cloud, there are considerable differences in the results from both techniques. Dense multi-view-stereo-matching provides 3D information for basically each image pixel at considerable quality if sufficient image overlap is available. However, the polar measurement principle of LiDAR sensors is advantageous whenever the object appearance changes rapidly when seen from different positions. This for example holds true for semi-transparent objects like vegetation, which is especially important for our application, which aims on the extraction of the bare earth for monitoring vegetated areas.

The Figure 2 also illustrates the high content of such dense point clouds. Here the meshed model from LiDAR points textured with UAV images is depicted.

The geometric accuracy evaluation is not considered here. Right now only results from one campaign are available, the second flight campaign from late fall 2018 is not completely processed yet. Thus monitoring itself is not yet possible. It is quite clear, that with a requested accuracy of better than 5 mm in object space, the limit of aerial mapping is close to reach. Current evaluation have shown that potential is left for refining the modelling of LiDAR and image data. In especially the combined adjustment of image and LiDAR seems to be straightforward. While matured hardware and software tools are available for point cloud generation from image matching and LiDAR, up to now both approaches were considered as competing techniques with research efforts focussing on the individual improvement of sensors and algorithms. In our future work, we will also aim on the suitable combination of both data sources to further increase robustness, accuracy and reliability of 3D point clouds while aiming at ultra-high precision applications from UAV-based data capture.

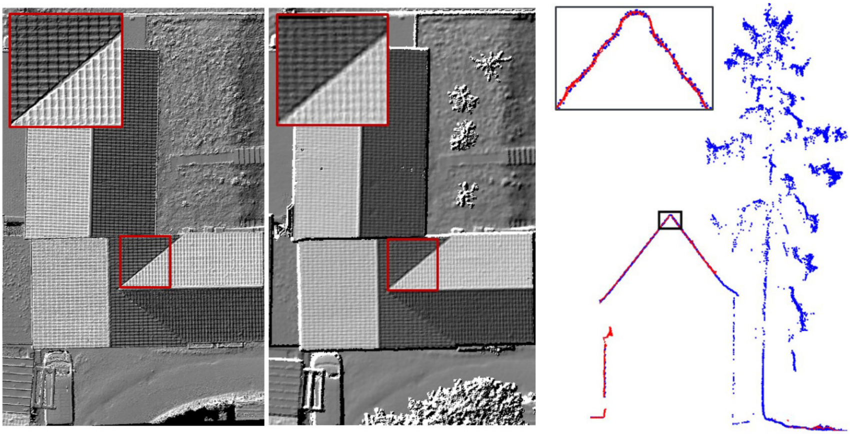

Figure 1: *Comparison between LiDAR point cloud and photogrammetric point cloud from dense image matching. Profile section (right) and shaded surface model from dense point image matching based on nadir imagery (left, grid width of DOM: 1 cm) and LiDAR (middle, grid width of DOM: 5 cm).*

Figure 2: *Meshed 3D surface model, based on LiDAR point cloud textured with (oblique) images acquired simultaneously with LiDAR measurement from the same UAV-platform.*

LiDAR_DIM: Integrated Capture and Evaluation of Airborne LiDAR and Imagery for High Precision 3D City Models

Until recently, Airborne LiDAR and Multi-View-Stereo-Matching (MVS) were considered as competing approaches for the generation of 3D point clouds. Thus, research efforts mainly focused on the individual improvement of these techniques. One main advantage of MVS is that the achievable geometric accuracy directly corresponds to the Ground Sampling Distance of the evaluated imagery. This allows 3D data capture at high resolutions even in the sub-centimeter range if a proper image scale is available. However, stereo image matching presumes the visibility of the respective object points in at least two images. This can become a problem for very complex 3D structures. Difficulties can arise for semi-transparent objects like vegetation or crane bars, for objects in motion like vehicles, pedestrians, etc., or in very narrow urban canyons. In contrast, the polar measurement principle of LiDAR sensors is advantageous whenever the object appearance changes rapidly when seen from different positions. Another advantage of LiDAR is the potential to measure multiple responses of the reflected signal.

The research project LiDAR_DIM is a cooperation between the companies IGI and nFrames and the Institute for Photogrammetry, University of Stuttgart, funded by the German Federal Ministry for Economic Affairs and Energy. It aims on the development of an integrated airborne camera and LiDAR system as well as an integrated data processing with the basic aim to generate high quality textured 3D meshes, which are enriched by semantic information.

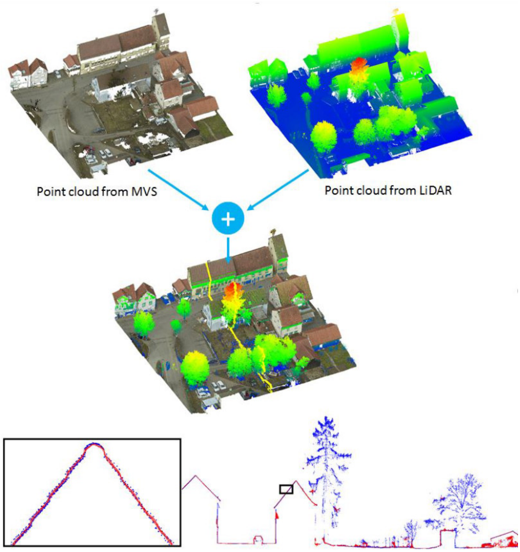

Figure 3: *Profile from joint cloud LiDAR (blue) and MVS (red).*

Feature Correspondences for Different Multi-Stereo Camera Configurations

Image orientation basically relies on the three steps feature extraction, feature matching and bundle adjustment. In order to compare two typical multi-stereo camera configurations for mobile mapping scenarios, we processed two rail datasets with our extended structure-from-motion procedure based on COLMAP and assessed the resulting tie point correspondences.

Both datasets were captured in train station areas and multi-stereo imagery was acquired from a locomotive in opposite driving directions. Both configurations feature a main stereo-vision system directed forward comprising 11 MP RGB cameras separated by a base of approx. 1 m. However, there is an additional forward pointing stereo system with 4 MP grayscale cameras for configuration I. Moreover, configuration I has three stereo systems with bases of ca. 80 cm comprising HD cameras, one facing downward to the rails and the others pointing right or left (see Figure 4). Dataset II used a standard Y configuration that additionally employs HD stereo cameras with bases of ca. 90 cm, which are directed back-right and back-left.

For dataset I, we considered a track section length of approx. 197 m leading to 98 and 87 timestamps, respectively. Since captured from ten industrial cameras, these 185 epochs resulted in 1850 images. Mean along-track distances between successive image exposures are 2.0 m and 2.3 m, respectively. COLMAP allowed a maximum distance between corresponding images of 20 m for feature matching. This resulted in a mean value of 2240 observations per image, even though images from the stereo system directed downward contain significantly fewer features. For dataset II consisting of 720 images, COLMAP computed an even smaller value of 1655 for mean observations per image. However, the principal reason are mean along-track spacings of 3.4 m (64 epochs) and 3.8 m (56 epochs), respectively.

Figure 4: *Left camera images from all stereo systems of configuration I captured at the same location.*

Figure 5 depicts 3D tie point connections after bundle adjustment, not only established between images of the same stereo camera system but also between imagery captured by different stereovision systems. Rows and columns represent all processed images in ascending order, from top to bottom and from left to right. Regarding the succession of forward RGB that is shown in the dashed gray square in the top left corner, there are first images captured by the left camera of the forward pointing system in direction 1, then in opposite direction 2, followed by imagery from the right camera in direction 1 and eventually right images in direction 2. Numbers of feature matches are color coded and a threshold of 30 defines the transition from red to blue.

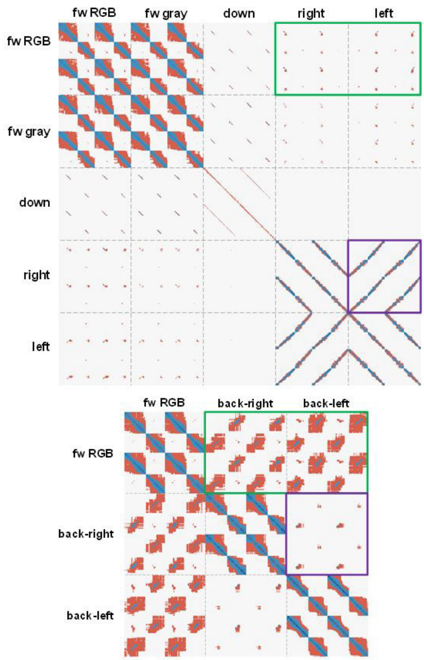

Figure 5: *Connectivity matrix for dataset I (top) and for dataset II captured with a standard Y stereo camera configuration (bottom). Colors represent tie point matches: from red that is up to 30 connections over to light blue until dark blue, which stands for several hundreds up to thousands of connections.*

Images recorded from forward facing cameras in the same driving direction have many connections, i.e. forward left and right but also forward RGB and gray. However, there are barely any connections between forward imagery captured from opposite driving directions. Some matches were obtained between images from the forward looking cameras and images from the cameras directed downward, right and left. Considering images from the downward pointing cameras, there are only a few connections between consecutive images of the same camera as well as between left and right camera images at the same epoch. The main reason are short distances to mapping objects such as rails, crossties and track ballast resulting in small acquired areas and small image overlapping, i.e. same points are seen in at most two consecutive images. Due to complementary mapped regions, there are no connections between downward facing imagery and images captured by the right as well as the left stereovision systems. Images from the right stereo camera system are well connected with images from the left stereo system captured in the opposite direction.

Furthermore, Figure 5 enables a comparison between stereo configuration I and standard Y stereo configuration II that is often used for road mapping. Configuration I allows only for a few tie points between the forward facing stereovision systems and the stereo camera systems directed right as well as left (see green rectangles). In contrast, imagery from the forward pointing stereovision system is well connected with images captured in the opposite direction from the systems looking back-right and back-left. The reasons are stereo system pointing differences of 90° for dataset I and ca. 45° for the standard Y configuration II. Still remarkable that several matches were established, since SIFT features often struggle with viewing direction differences of more than 30°. On the other hand, many more SIFT features can be matched between stereovision systems pointing right and left compared to stereovision systems facing back-right and back-left (see purple squares). While left and right images from opposite driving directions have approximately the same viewing direction, there is a difference of around 90° between back-right and back-left stereo camera systems.

DSM and Point Cloud Generation with very high Resolution Multi-view Stereo Satellite Imagery

In 2016, a well-organized multi-view stereo benchmark for commercial satellite imagery has been released by the John Hopkins University Applied Physics Laboratory (JHU/APL), USA. The JHU/APL benchmark contains fifty WorldView-3 panchromatic images. These MVS images were collected from November 2014 to January 2016. The test site of the benchmark is close to San Fernando, Argentina. The GSD of the dataset varies from 30cm to 50cm, according to the off-nadir angle. The lidar point cloud and the digital suface model (DSM) at 20cm GSD are provided as reference data. This benchmark motivated us to explore methods, which can generate accurate digital surface models from a large number of high resolution satellite images.

We propose a binocular pipeline for the processing of MVS high resolution satellite imagery, which is shown in Figure 6.

The MVS satellite images were collected at different dates. The differences of the satellite's geometric configurations, atmosphere conditions, and illumination situation affects the quality of the results. Therefore, an image pair selection is needed as pre-processing. According to our experiments, we apply an image selection strategy as follows:

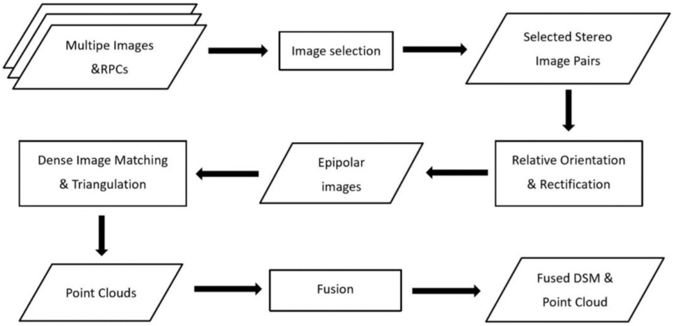

Figure 6: *DSM Generation Pipeline of MVS high resolution satellite imagery.*

- Eliminate images that have an incidence angle larger than 35 degrees
- Divide the remaining images into a winter and summer group
- Order the images by month
- Select the images that are collected in the same month
- Choose the image pairs having an intersection angle between 5 and 35 degrees

Since there are no ground control points (GCPs) in the test sites, a relative orientation is calculated to refine the Rational Polynomial Coefficients (RPCs). One stereo image pair is selected to calculate a quasi ground truth surface. The corresponding quasi-GCPs of the tie points are calculated by forward intersection with the raw RPCs. Then, a RPC bundle block adjustment is applied. All stereo image pairs are aligned to the quasi ground truth surface. Next, the selected image pairs and the refined RPCs are applied to generate the epipolar image pairs, so that the corresponding points are located on the same line in image space. After this image rectification, a modified tube-based Semi-Global Matching (tSGM) is used for every stereo pair. The point clouds are generated via forward intersection according to the matching result. A median filter is applied for the fusion of the point clouds. The fused point cloud is then converted into a grid (in UTM coordinate system) to generate the fused DSM (Figure 7(a)).

In order to verify the quality of the fused DSM, we compare the height differences between the fused DSM and the reference LiDAR DSM (Figure 7(b)). The RMSE and the median errors of the height differences are evaluated for the accuracy computation. The completeness is the percentage of the points which have less than 1 m height difference to the ground truth. Moreover, we compute the normalized median deviation (NMAD) and the 68% and 95% quantiles of the absolute errors to evaluate the robustness of the fused DSM. Before the final evaluation, we need to find a proper number of input point clouds for the fusion, because the quality of the fused DSM will improve with more inputs, but will get worse if more low quality point clouds are applied. The point clouds are sorted by the completeness. Applying point clouds from high to low quality, we generate the fused result with different input numbers. The relation between the input point clouds and the completeness of the fused result is shown in Figure 8. According to our experiments, we find the peak would be ca. 30 point clouds. If more point clouds are used, the completeness of the fused point cloud and DSM decrease. Therefore, 30 point clouds would be a proper number in this test site. The statistical evaluation result of the fused DSM with 30 inputs is shown in Table 1. Although the image are collected at different dates, our pipeline is able to generate high quality point clouds and DSMs from the MVS high resolution imagery.

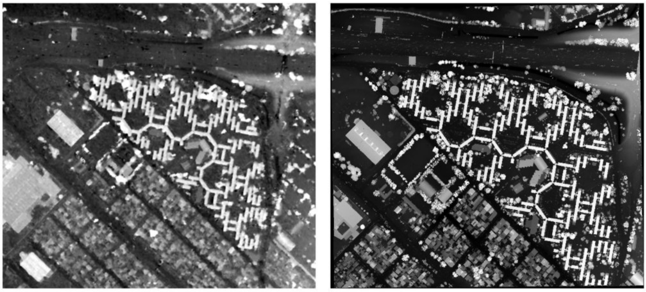

(a) (b)

Figure 7: *DSM of (a) MVS high resolution satellite imagery; (b) reference Lidar data.*

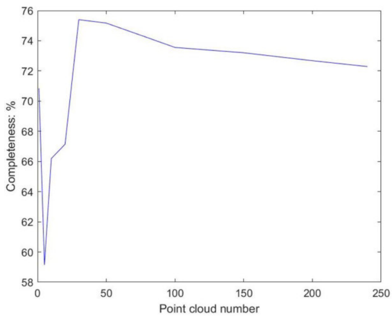

Figure 8: *The relation between the number of fused point clouds and the completeness.*

Table 1: *Evaluation result of fused DSM.*

Mean Error (m)	RMSE (m)	Completeness (%)	NMAD (m)	Aq68 (m)	Aq95 (m)
0.320	2.702	75.40	0.503	0.660	5.930

Bathymetry by Fusion of Airborne Laser Scanning and multi-spectral Aerial Imagery

In the second year of the DFG research project *Bathymetry by fusion of airborne laser scanning and multi-spectral aerial imagery*, the research work concentrated on:

- additional data acquisitions to provide optimal datasets for the research on bathymetry via active and passive optical remote sensing
- deriving bathymetry from through-water Dense Image Matching
- deriving bathymetry from multispectral images
- dissemination of the achieved research results
- proposal for 12 month project extension

For each of the topics mentioned above, a more detailed description is provided in the following:

Data acquisition

As it turned out that the LiDAR (Light Detection and Ranging) and image data captured in August 2017 in the Stubai valley, Tyrol, Austria (cf. annual report 2017), was not fit for purpose due to unfavorable environmental conditions caused by heavy thunderstorms prior to the airborne data acquisition, a new experiment was planned in early 2018. The IfP hereby teamed up with the companies *Integrated Geospatial Innovations* (IGI), Kreuztal, Germany, and *Airborne Hydro Mapping* (AHM), Innsbruck, Austria. IGI provided two 100 MPixel PhaseOne cameras (RGB+Coastal blue). AHM conducted the flight and provided a topo-bathymetric laser scanner. All in all, around a dozen freshwater lakes and a portion of the Lech River were captured around Augsburg, Germany. The specific aim of the experiment was to investigate the benefit of a high-resolution water penetrating coastal blue channel (λ=400-460nm) for deriving bathymetry via photogrammetry and spectrally based image analysis. The camera integration and the flight strip overview are displayed in Figure 9.

Bathymetry via through-water dense image matching

One of the core topics of the DFG research project is the derivation of bathymetry via two-media photogrammetry. In-depth research was carried out to make use of state-of-the-art Dense Image Matching (DIM) techniques in the two-media (air-water) environment. The added complexity hereby is the image ray refraction at the air-water-interface, which causes an underestimation of the water depth in the raw measurements. Appropriate correction models for the multi-view stereo case, typically used for DIM, were derived and implemented in the course of the project. Good results were achieved for Lake Autobahnsee (cf. Figure 10).

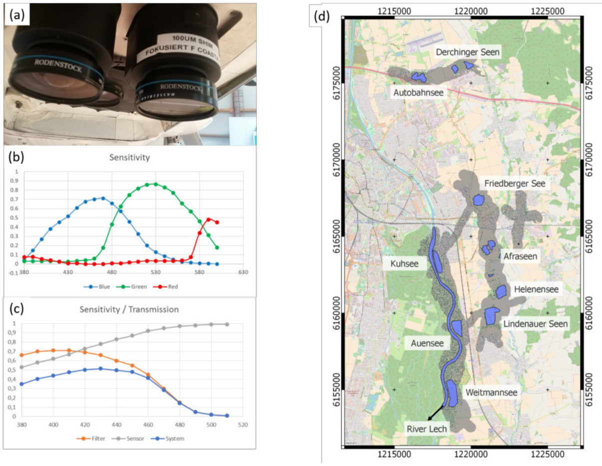

Figure 9: *Data acquisition Augsburg, April, 2018: (a) PhaseOne RGB and Coastal Blue cameras, (b) Sensitivity curves for RGB channels, (c) sensitivity and tranmission curves for Coastal Blue channel, (d) Study area around Augsburg.*

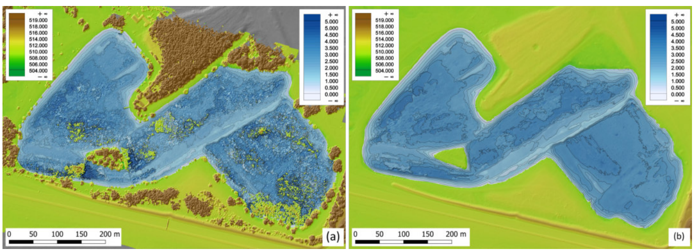

Figure 10: *Lake Autobahnsee, Augsburg, Germany; (a) Digital Elevation Model from through-water Dense Image matching (multi-view stereo matching), (b) Digital Terrain Model LiDAR.*

Bathymetry from multispectral images

In parallel to two-media photogrammetry, a further research focus was on spectrally based bathymetry. Hereby, the depths are estimated from the radiometric image content by establishing a relation between image gray values and depth based on ground truth data. The reference data used in our project either stemmed from echo sounding (Grünausee, Blaue Lacke, Stubai valley) or from concurrent airborne laser bathymetry (Autobahnsee, Augsburg, Germany). Although research in this area is still ongoing, first results were already obtained for both datasets mentioned above. Figure 11 shows a respective example.

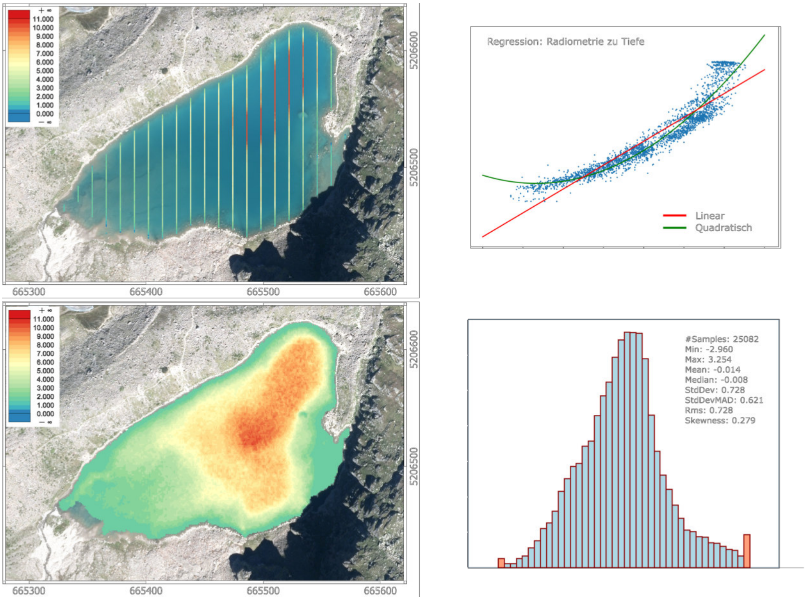

Figure 11: *Grünausee, Stubai valley, Tyrol, Austria. Top row: (left) RGB mosaic overlaid with echo sounding depth profiles (colour coded); (right) regression radiometric: quantity x=ln(blue/green) vs. depth. Bottom row: (left) spectrally based depth map; (right) histogram of nominal-actual height deviations.*

Applying Semantics to Meshed Models of Urban Scenes

Virtual City Models are an integral part of our daily lives. Applications like navigation, urban planning and computer games base on 2D and 3D geodata. These applications mainly focus on geometric information and take semantics as additional information. Recently, however, semantic information, automatically derived from the captured data itself, becomes more and more important for a convincing representation of the real world.

Deep learning (DL) methods have become the standard technique in 2D computer vision tasks. We leverage these methods in order to classify buildings within geolocated imagery. To that end, we train a Convolutional Neural Network (CNN) for classifying street-view images of building facades into five use classes. The classes *commercial* and *residential* represent a singular use of a building, while the class *hybrid* represents a mixture of these two use classes. The class *specialUse* represents the remaining buildings not matching the other three classes, like e.g. schools and churches. Finally, the class *underConstruction* contains buildings being under construction independently on their actual use. Due to the usage of geolocated imagery the predictions can be mapped onto a mesh representation in a further step.

With the help of so-called Class Activation Maps (CAMs) learned features can be localized and interpreted within input images. CAMs are heat maps that highlight image sections, which are decisive for the respective prediction. Thereof, a human operator can derive learned features, which are useful for understanding the networks decisions. Figure 12 shows correctly classified images and misclassified images overlaid by the associated CAMs.

Figure 12: *Top row: Correct classifications of a CNN with overlaid CAMs. Bottom row: Misclassifications. The red spots highlight the most decisive image parts.*

Despite their success in image space, DL methods are not yet state-of-the-art for 3D data representations like point clouds or meshes. In photogrammetry and remote sensing, however, these kinds of data are very common. Nowadays, textured triangle meshes are the standard representation of virtual city models for 2.5D and 3D geodata. To the best of our knowledge, little work focuses on utilizing DL for semantic mesh segmentation yet. In general, little effort is put into semantic mesh segmentation in urban scenes. This is because there are no benchmark data sets for semantic mesh segmentation of urban scenes. For this reason, we create our own ground truth data, which consists of real-world textured meshes and synthetic data from procedural modelling. To that end, we create a hybrid data set consisting of real-world and synthetic data in order to train a multi-branch 1D CNN approach.

Our real-world data covers a monitoring site in Hessigheim. The data was captured in collaboration with the BfG with a Riegl VUX -1LR LiDAR combined with two oblique Sony Alpha 6000 cameras. We created a 2.5D triangle mesh based on LiDAR measurements with the software SURE by nFrames. The generated mesh (750m x 300m) is textured using oblique imagery. As labelling is a very tedious and time-consuming task, we additionally leverage the synthetic SynthCity data set. The annotated classes of our ground truth are inspired by the ISPRS 3D Semantic Labeling Contest: *building mass/facade, roof, impervious surface, green space, mid and high vegetation, vehicle, waterbody, chimney/antenna* and *clutter*. The classes *building mass/facade* and *roof* are chosen to be mutually exclusive, since roof extraction is a quite common task. *Impervious surface* includes streets, sidewalks, parking lots and other man-made surfaces. To give an illustration, Figure 13 shows a small subset of the textured and manually labelled 2.5D mesh.

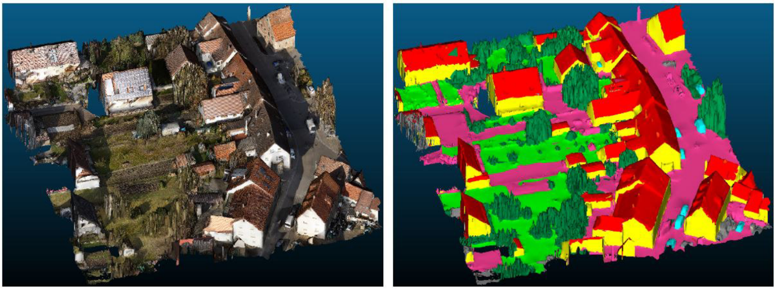

Figure 13: *A 100m x 100m tile of the textured (left) and manually labelled (right) 2.5D mesh of Hessigheim. Light green: green space, dark green: mid and high vegetation, red: roof, yellow: building mass/facade; magenta: impervious surface, blue: vehicle, black: clutter.*

For each mesh face, multi-scale geometric and textural features are computed and serve as input for the respective branches of the multi-branch 1D CNN. Figure 14 visualizes some features. Ordinarily, neural networks are an end-to-end learning approach operating on regularly structured input data like images or voxel space. Meshes, however, consist of arbitrarily shaped faces and therefore they are not regularly structured. Hence, we calculate a multi-scale feature vector for each face and can thereby consider them as data points as usual in machine learning. To put it another way, we leverage feature engineering in order to make use of CNNs. This is somehow levering out the idea of end-to-end learning wherefore we denote this as a hybrid model. The gist of this approach is to create data points out of the irregularly shaped mesh in order to make it applicable to the 1D CNN. Moreover, this approach can be applied to different data representations while utilizing representation-specific properties: data can be two-dimensional or three-dimensional; data can be regularly shaped or irregularly shaped.

By utilizing the results of our building classification in image space, we can attach a fine-grained classification to the segments predicted as *building mass/facade* by our semantic mesh segmentation pipeline. This depicts an important step towards the holistic interpretation of urban data.

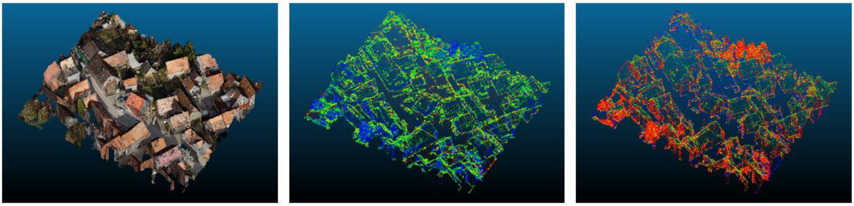

Figure 14: *Textured Tile (left) and visualized features for a subset of faces: horizontality (center) and verticality (right). Color scale: blue (low value) to red (high value).*

ALS Point Cloud Classification with Submanifold Sparse Convolutional Neural Networks

Semantic segmentation of point clouds is usually one of the main steps in automated processing of data from Airborne Laser Scanning (ALS). Established methods usually require expensive calculation of handcrafted, point-wise features. In contrast, Convolutional Neural Networks (CNNs) have been established as powerful classifiers, which at the same time also learn a set of optimal features by themselves. However, their application to ALS data is not trivial. Pure 3D CNNs require a lot of memory and computing time, therefore most approaches project point clouds into two-dimensional images.

Sparse Submanifold Convolutional Networks (SSCNs) address this issue by exploiting the sparsity often inherent in 3D data. We investigate the application of SSCNs for efficient semantic segmentation of ALS voxel clouds in an end-to-end encoder-decoder architecture. We evaluate this method on the ISPRS Vaihingen 3D Semantic Labeling benchmark and achieving state-of-the-art accuracies. Furthermore, we experiment with large-scale ALS data using the example of the Actueel Hoogtebestand Nederland (AHN3).

The achieved overall accuracy on the ISPRS Vaihingen 3D Benchmark is state-of-the-art. Rare object categories can still be identified reasonably well when trained with a weighted loss function, given their inner class variance is well represented in the training set. The implicit geometry of the point cloud has proven to be the primary feature. Difficult classes in the ISPRS Vaihingen 3D dataset are in particular shrubs and hedges or fences, which are often interpreted as various types of vegetation. Low vegetation and impervious surfaces are prone to confusion due to their similar geometry. Larger amounts of ALS training data like the AHN3 dataset make training more stable and achieve better test results. However, these networks still requires a considerable amount of graphics memory, limiting resolution and sample extent.

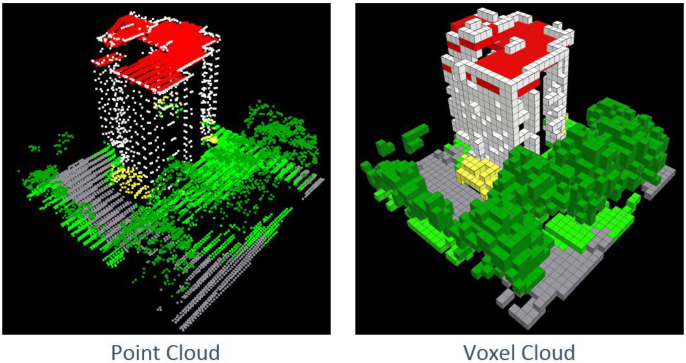

Figure 15: *Point clouds need to be voxelized for processing in CCNs. However, instead of a dense voxel grid, for SCCNs a list of non-empty voxels is sufficient. Voxel attributes like intensity are obtained by averaging over the included points of each voxel.*

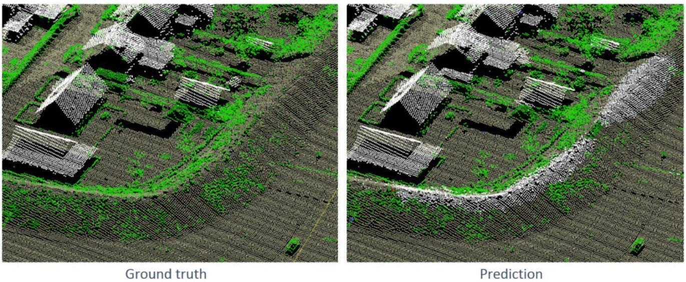

Figure 16: *Examples of AHN3 points, predicted at 0.25m voxel resolution. Green: unassigned; brown-gray: ground; white: buildings; blue: water; red: bridges.*

mDBSCAN: Real Time Superpixel Segmentation by DBSCAN Clustering based On Boundary Term

In these days, superpixels have a great interest in the field of computer vision and image processing. They have been widely applied in image segmentation, 3D reconstruction, scene flow and object tracking. A superpixel is a set of pixels that share the same features, for example, color information, texture features, and others. Superpixel algorithms are performed as a pre-processing step in many computer vision applications in order to reduce the computational time of subsequent processing without affecting the performance of the entire system. Therefore, fast computation superpixel algorithms that provide high boundary adherence and segmentation accuracy are preferred. Many superpixel algorithms have been introduced such as Simple Linear Iterative Clustering (SLIC), Entropy Rate Superpixel Segmentation (ERS), Superpixels Extracted via Energy-Driven Sampling (SEEDS), and DBSCAN.

Different approaches have been followed to generate superpixels, for example, SLIC deals with superpixels as an iterative clustering problem. On the other hand, SEEDS considers the superpixels as an energy maximization problem, which achieved a good boundary adherence. Our approach deals with superpixels as a non-iterative clustering problem. Moreover, it presents precisely the boundary adherence by defining a novel simple distance measurement that considers the boundary information as well as the color and spatial information between the superpixel and its neighbors. All of the approaches are aiming to fulfill the requirements of superpixels by having regular, compact and connected superpixels with high boundary adherence and low computational complexity. Figure 17 shows the superpixel results of the modified DBSCAN algorithm (mDBSCAN) that have compact and regular shapes, which precisely represent the image boundaries.

Figure 17: *Image segmentation using mDBSCAN algorithm. The number of superpixels are 250, 500 and 1000, respectively.*

mDBSCAN is an improved version of DBSCAN (Density Based Spatial Clustering of Applications with Noise) superpixel segmentation. The proposed algorithm has an automatic threshold based on the color and gradient information. The proposed algorithm performs under different color space such as RGB, Lab and grey images using a novel distance measurement. The distance combines three terms i.e., normalized spatial information, gradient information, and weighted color information. The experimental results demonstrate that the proposed algorithm outperforms the state of the art algorithms in terms of boundary adherence and segmentation accuracy with low computational cost (30 frames/s) as shown in figure 18.

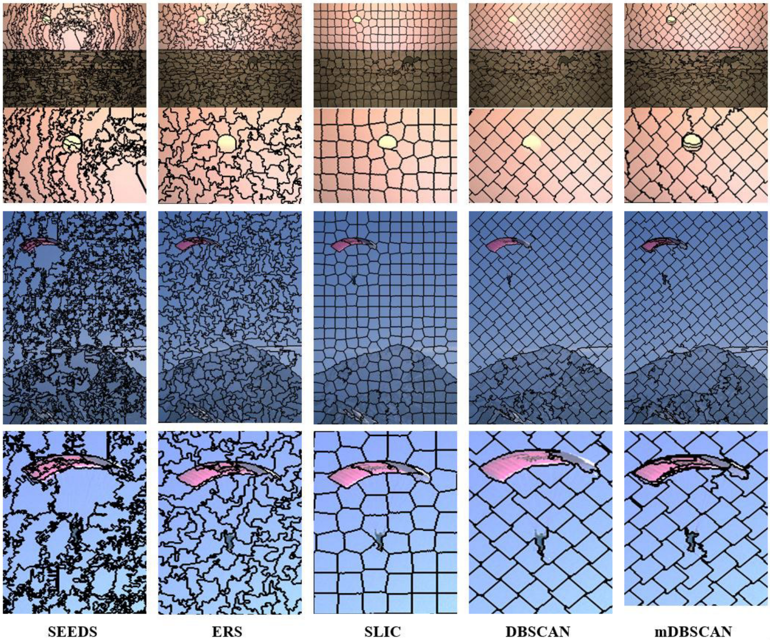

Figure 18: *Visual comparison of superpixel segmentation results. The average number of superpixels is roughly 300.*

References 2018

Abdelaal, M., Reichelt, D., Dürr, F., Rothermel, K., Runceanu, L., Becker, S., Fritsch, D.: ComNSense: Grammar-Driven Crowd-Sourcing of Point Clouds for Automatic Indoor Mapping. Proceedings of the ACM on Interactive, Mobile, Wearable and Ubiquitous Technologies, 2(1), Article No. 1, 26 p.

Blaser, S., Cavegn, S., Nebiker, S.: Development of a Portable High Performance Mobile Mapping System Using the Robot Operating System. ISPRS Ann. Photogramm. Remote SenSpatial Inf. Sci., IV-1, 13-20.

Blaser, S., Nebiker, S., Cavegn, S.: On a Novel 360 degree Panoramic Stereo Mobile Mapping System. Photogrammetric Engineering, Remote Sensing, 84(6), 347-356.

Cavegn, S., Blaser, S., Nebiker, S., Haala, N.: Robust and Accurate Image-based Georeferencing Exploiting Relative Orientation Constraint. ISPRS Ann. Photogramm. Remote SenSpatial Inf. Sci., IV-2, 57-64.

Cramer, M., Haala, N., Laupheimer, D., Mandlburger, G., Havel, P.: Ultra-high precision UAV-based LiDAR and Dense Image Matching. Int. Arch. Photogramm. Remote SenSpatial Inf. Sci., XLII-1, 115-120.

Gruber, T., Kokhova, M., Ritter, W., Haala, N., Dietmayer, K.: Learning Super-resolved Depth from Active Gated Imaging. 21st IEEE International Conference on Intelligent Transportation Systems (IEEE ITSC 2018).

Gu, H., Han, Y., Yang, Y., Li, H., Liu, Z., Sörgel, U., Blaschke, T., Cui, S.: An Efficient Parallel Multi-Scale Segmentation Method for Remote Sensing Imagery. Remote Sensing 10(4), 590.

Jhan, J.-P., Rau, J-Y., Haala, N.: Robust and adaptive band-to-band image transform of UAS miniature multi-lens multispectral camera. ISPRS Journal of Photogrammetry and Remote Sensing 137, 47-60.

Kenduiywo, B. K., Bargiel, D., Sörgel, U.: Crop-type mapping from a sequence of Sentinel 1 images. International Journal of Remote Sensing 39(19), 6383-6404.

Laupheimer, D, Haala, N.: Deep Learning for the Classification of Building Facades. Publikationen der DGPF, Band 27, 701-709.

Laupheimer, D., Tutzauer, P., Haala, N., Spicker, M.: Neural Networks for the Classification of Building-use from Street-View Imagery. ISPRS Ann. Photogramm. Remote SenSpatial Inf. Sci., IV-2, 177-184.

Li, H., Ghamisi, P., Sörgel, U., Zhu, X.: Hyperspectral and LiDAR Fusion Using Deep Three-Stream Convolutional Neural Network. Remote Sensing 10(4), 1649.

Lotte, R.G., Haala, N., Karpina, M., Aragao, L.E.O.C., Shimabukuro, Y.E.: 3D Facade Labeling over Complex Scenarios: A Case Study Using Convolutional Neural Network and Structure-From-Motion. Remote Sensing 10(4), 1435.

Mandlburger, G.: Gewässervermessung mittels aktiver und passiver optischer Fernerkundung. Vermessung und Geoinformation 3/2018, 195-206.

Mandlburger, G.: A review of Airborne Laser Bathymetry sensor. In: Proc. of the 5th IAHR Europe Congress - New Challenges in Hydraulic Research and Engineering, 41-42.

Mandlburger, G.: A Case Study on Through-Water Dense Image Matching. Int. Arch. Photogramm. Remote SenSpatial Inf. Sci., XLII-2, 659-666.

Mandlburger, G.: Topography and Bathymetry via Laser Scanning and Multi-Spectral Imaging - From Sensors to Application. Tutorial at the ISPRS TC I Symposium in Karlsruhe 2018.

Mandlburger, G., Jutzi, B.: Feasibility Investigation on Single Photon LiDAR Based Water Surface Mapping. ISPRS Ann. Photogramm. Remote SenSpatial Inf. Sci., IV-1, 109-116.

Mandlburger, G., Kremer, J., Steinbacher, F., Baran, R.: Investigating the Use of Coastal Blue Imagery for Bathymetric Mapping of Inland Water BodieInt. Arch. Photogramm. Remote SenSpatial Inf. Sci., XLII-1, 275-282.

Meißner, H., Cramer, M., Reulke, R.: Towards Standardized Evaluation of Image Quality for Airborne Camera System. Int. Arch. Photogramm. Remote SenSpatial Inf. Sci., XLII-1, 295-300.

Meißner, H., Przybilla, H.-J., Cramer, M., Stebner, K.: UAV-Kameras - Bewertung von Kalibrierung, Langzeitstabilität und optischem Auflösungsvermögen. Beiträge zum 169. DVW-Seminar UAV 2018 - Vermessung mit unbemannten Flugsystemen, 19.-20. Februar 2018 in Hamburg, Schriftenreihe des DVW-Gesellschaft für Geodäsie, Geoinformation und Landmanagement e.V., Band 89/2018, Wißner Verlag, 47-59.

Milenkovic, M., Ressl, C., Karel, W., Mandlburger, G., Pfeifer, N.: Roughness Spectra Derived from Multi-Scale LiDAR Point Clouds of a Gravel Surface: A Comparison and Sensitivity Analysis. ISPRS Int. J. Geo-Inf., 7, 69.

Rettenmund, D., Fehr, M., Cavegn, S., Nebiker, S.: Accurate Visual Localization in Outdoor and Indoor Environments Exploiting 3D Image Spaces as Spatial Reference. Int. Arch. Photogramm. Remote SenSpatial Inf. Sci., XLII-1, 355-362.

Runceanu, L.S., Haala, N.: Indoor Mesh Classification for BIM. Int. Arch. Photogramm. Remote SenSpatial Inf. Sci., XLII-4, 535-539.

Schilling, H., Bulatov, D., Niessner, R., Middelmann W. and Sörgel, U.: Detection of Vehicles in Multisensor Data via Multibranch Convolutional Neural Network. IEEE Journal of Selected Topics in Applied Earth Observations and Remote Sensing, 11, 4299-4316.

Walter, V.: Integration of multiple collected polygons with a raster-based approach. Int. Arch. Photogramm. Remote SenSpatial Inf. Sci., XLII-4, 679-685.

Walter, V., Sörgel, U.: Results and Problems of paid Crowd-based geospatial Data Collection. PFG Journal of Photogrammetry, Remote Sensing and Geoinformation Science, 86(3-4), 87-197.

Master Theses

Akerele, A.H.: On the Role of Image Quality in Photogrammetric Processing - an Empirical Study. Supervisor: Cramer, M.

Ayyad, R.: Comparison of Persistent Scatterer Interferometry Results using TerraSAR-X and Sentinel-1 Images. Supervisor: Sörgel, U., Yang, C.H.

Blackler, H.: Erfassung und Georeferenzierung von Bilddaten für die Erkennung von Pflanzen in landwirtschaftlichen Anwendungen. Supervisors: Haala, N., Cramer, M., Reiser, D. (Uni Hohenheim).

Bolz, T.: Automatisierte objektbasierte Degradationsklassifikation für Radarsensoren. Supervisors: Sörgel, U., Männicke, N. (Robert Bosch GmbH).

Ehmke, S.: Qualifizierung von Sensoren zur Kollisionsvermeidung beim automatisierten Fahren. Supervisors: Schuler, B. (Daimler AG), Haala, N.

Fischer, J.: Georeferenzierung von UAV-Befliegungen durch terrestrisches LIDAR. Supervisor: Cramer, M.

Gorska, J.D.: POI Match Review - elimination of duplicates by applying automated classifier. Supervisors: Walter, V., Adetutu, E. (HERE Technologies), Prieto, A. (HERE Technologies), Rybalchenko, G. (HERE Technologies).

Hajer, L.: Auslegung und Erprobung eines reflexbasierten Verfahrens zur Charakterisierung von Heliostaten. Supervisors: Jessen, W., Prahl, C., Haala, N.

Immel, T.: Analyse von Wettereinflüssen auf LiDAR-Sensoren für autonomes Fahren. Supervisors: Heinzler, R. (Daimler AG), Haala, N.

Jia, W.: Mapping and Localization Based on High Resolution Automotive Radar. Supervisors: Haala, N., Li, M. (Robert Bosch GmbH).

Jumadi, J.: WebGIS for Visualization and Spatial Analysis of Cadastral Information System using Open Source Software. Supervisor: Walter, V.

Kohler, S.: 3D-Unkrauterkennung für Echtzeitverfahren in der Landwirtschaft. Supervisors: Reiser, D. (Uni Hohenheim), Schmohl, S.

Kokhova, M.: Learning Super-resolved Depth from Multiple Overlapping Gated Images with Neural Networks. Supervisors: Gruber, T. (Daimler AG), Haala, N.

Kölle, M.: Klassifikation hochaufgelöster LiDAR- und MVS-Punktwolken zu Monitoringzwecken. Supervisors: Haala, N., Laupheimer, D.

Li, H.: Composite Kernels for Multisensor Image Cassification. Supervisors: Sörgel, U., Zhu, X., Ghamisi, P.

Li, Y.: Comparison between PSI and SBAS monitoring - a case study of city subsidence caused by tunnel construction. Supervisors: Sörgel, U., Yang, C.H.

Lian, Z.: Digital Preservation of Calw Market Square-Lederstrasse by Means of Automated HDS and Photogrammetric Texture Mapping. Supervisor: Fritsch, D.

Schneider, P.: Klassifikation von Verkehrsteilnehmern in FMCW-RADAR Mikro-Doppler Signaturen mittels CNN, basierend auf simulierten und realen Trainingsdaten. Supervisors: Stolz, M. (Robert Bosch GmbH), Haala, N.

Sheu, C.Y.: Automatic 3D lane marking reconstruction using multi-view aerial imagery. Supervisors: Kurz, F. (DLR), Haala, N.

Shoushtari, M.H.: Modeling and Prediction of On-Street Parking Spaces Using Geospatial Analytics. Supervisor: Walter, V.

Wiedemann, A.: Intelligent Analysis and Creation of Training Data for Simple Object Detectors based on Convolutional Neural Networks. Supervisors: Haala, N., Richter, F. (Robert Bosch GmbH).

Zhan, K.: Dynamic and Accurate Image Feature Extraction for Camera Calibration. Supervisors: Küver, M., Shahraki, M. (Robert Bosch GmbH), Haala, N.

Bachelor Theses

Collmar, D.: Erstellung einer GUI zur crowd-basierten Digitalisierung von Objekten sowie Analyse der dadurch erhaltenen Daten. Supervisor: Walter, V.

Lorenz, F.: Untersuchung von Verfahren zur web-basierten Bildersuche und Kartenerkennung. Supervisor: Walter, V.

Shiller, I.: Entzerrung von Infrarot- sowie CCD-Aufnahmen zur Messung von Oberflächentemperaturen. Supervisors: Brack, S., Haala, N.

Stelzer, R.: Entwicklung eines Webinterfaces zum crowd-basierten Vergleich der Kartendienste OpenStreetMap und Maps4BW. Supervisor: Walter, V.

Activities in National and International Organizations

Cramer, M.:

Co-Chair ISPRS WG I/9: Integrated Sensor Orientation, Calibration, Navigation and Mapping

Mitglied im DIN Normungsausschuss NA 005-03-02 AA “Photogrammetrie und Fernerkundung”

Englich, M.:

Webmaster ISPRS

Haala, N.:

Chair ISPRS WG II/2: Point Cloud Beneration

Vorsitz DGPF Arbeitskreis Sensorik und Plattformen

Sörgel, U.:

Vice President German Society for Photogrammetry, Remote Sensing and Geoinformation (DGPF)

Chair ISPRS WG III/3: SAR-Based Surface Generation and Deformation Monitoring

Walter, V.:

National Correspondent of the ISPRS Commission IV

Education - Lectures/Exercises/Training/Seminars

Bachelor “Geodäsie und Geoinformatik”

Geoinformatics I (Walter)	2/2/0/0
Geoinformatics II (Walter)	1/1/0/0
Image Processing (Haala)	2/1/0/0
Integrated Fieldworks (Haala, Keller, Kleusberg, Sneeuw)	0/0/4/0
Introduction into Geodesy and Geoinformatics (Cramer, Keller, Kleusberg, Sörgel, Sneeuw)	4/2/0/0
Photogrammetry (Cramer)	2/1/0/0
Remote Sensing (Sörgel)	2/1/0/0
Signal Processing (Sörgel)	2/1/0/0
Urban Planning (Dvorak)	2/0/0/0

Master Course “Geodäsie und Geoinformatik”

Aerotriangulation (Cramer)	1/1/0/0
Computational Geometry (Walter)	1/1/0/0
Computer Vision for Image-based Acquisition of Geodata (Haala)	1/1/0/0
Databases and Geographical Information Systems (Walter)	1/1/0/0
Digital Terrain Models (Haala)	1/1/0/0
Fundamentals in Urban Planning (Dvorak)	2/0/0/0
Georeferencing of photogrammetric Systems (Cramer)	1/1/0/0
Modelling and Visualisation (Haala)	1/1/0/0
Pattern Recognition and Image Understanding (Haala)	1/1/0/0
Remote Sensing (Sörgel)	1/1/0/0
Scientific Presentation Seminar (Haala)	0/0/0/2
Topology and Optimisation (Becker)	1/1/0/0
Web-based GIS (Walter)	1/1/0/0

Master Course GEOENGINE

Airborne Data Acquisition (Cramer)	2/1/0/0
Geoinformatics (Walter)	2/2/0/0
Signal Processing (Sörgel)	2/1/0/0
Image-based Data Collection (Haala, Cramer)	2/1/0/0
Integrated Fieldworks (Haala, Sneeuw, Keller, Kleusberg)	0/0/4/0
Remote Sensing (Sörgel)	2/1/0/0
Topology and Optimisation (Becker)	2/1/0/0

Master Course “Infrastructure Planning”

Introduction to GIS (Walter)	2/0/0/0

Master Course “Aerospace Engineering”

Image Processing (Haala)	2/1/0/0
Introduction into projective Geometry (Cramer)	2/0/0/0